



**HAL**  
open science

# Influence of biogenic NO emissions from soil on Atmospheric chemistry over Africa: a regional modelling study

Eric Martial Yao, Fabien Solmon, Marcellin Adon, Claire Delon, Corinne Galy-Lacaux, Graziano Giuliani, Bastien Sauvage, Véronique Yoboue

## ► To cite this version:

Eric Martial Yao, Fabien Solmon, Marcellin Adon, Claire Delon, Corinne Galy-Lacaux, et al.. Influence of biogenic NO emissions from soil on Atmospheric chemistry over Africa: a regional modelling study. EGU sphere, 2025, 10.5194/egusphere-2024-3179 . hal-04934981

**HAL Id: hal-04934981**

**<https://hal.science/hal-04934981v1>**

Submitted on 7 Feb 2025

**HAL** is a multi-disciplinary open access archive for the deposit and dissemination of scientific research documents, whether they are published or not. The documents may come from teaching and research institutions in France or abroad, or from public or private research centers.

L'archive ouverte pluridisciplinaire **HAL**, est destinée au dépôt et à la diffusion de documents scientifiques de niveau recherche, publiés ou non, émanant des établissements d'enseignement et de recherche français ou étrangers, des laboratoires publics ou privés.



Distributed under a Creative Commons Attribution 4.0 International License



# Influence of biogenic NO emissions from soil on Atmospheric chemistry over Africa: a regional modelling study

Eric Martial YAO<sup>1,2</sup>, Fabien Solmon<sup>2</sup>, Marcelin ADON<sup>1</sup>, Claire DELON<sup>2</sup>, Corinne GALY-LACAU<sup>2</sup>, Graziano GIULIANI<sup>3</sup>, Bastien SAUVAGE<sup>2</sup>, and Véronique YOBOUE<sup>4</sup>

<sup>1</sup>Laboratoire des Sciences et Technologies de l'Environnement, Université Jean Lorougnon Guédé, Daloa, Côte d'Ivoire.

<sup>2</sup>Laboratoire d'Aérologie, Université Paul Sabatier Toulouse III, CNRS, IRD, 14 Avenue Edouard Belin 31400 Toulouse, France.

<sup>3</sup>Earth System Physics Section, International Centre for Theoretical Physics, 34151 Trieste, Italy.

<sup>4</sup>Laboratoire des Sciences de la Matière, de l'Environnement et de l'Energie Solaire, Université Félix Houphouët-Boigny, Abidjan, Côte d'Ivoire.

**Correspondence:** Eric Martial YAO (yaoeric0746@gmail.com) and Fabien SOLMON (fabien.solmon@aero.obs-mip.fr)

**Abstract.** In the context of climate change and increasing anthropogenic pressures in Africa, understanding the interactions between atmospheric chemistry, regional climate, and biogeochemical cycles is critical. This study investigates the potential role of biogenic nitric oxide emissions from African soils (BioNO), particularly in arid and semi-arid ecosystems, as significant contributors to atmospheric NO<sub>2</sub> emissions and regional atmospheric chemistry. To this end, we rely on a modelling approach based on the RegCM5 regional climate model, including an updated atmospheric chemistry module and, amongst other, a specific parametrization for BioNO emissions. Throughout the paper, the model performances are evaluated against various datasets including in-situ observations from the INDAAF network and chemical reanalyses. Sensitivity studies demonstrate that integrating BioNO emissions into the model enhances the accuracy of simulated NO<sub>2</sub>, HNO<sub>3</sub>, and O<sub>3</sub> seasonal cycles and surface concentration magnitudes, while reducing simulated biases against ground based observations. Large differences are however still present regarding notably the simulated surface ozone concentration magnitude vs in situ measurements, while these biases are also observed for chemical reanalyses, and a state of the art chemistry transport model used for comparison. Beside outlining the impact and added value of BioNO flux representation for regional atmospheric chemistry, our findings also outline the suitability of RegCM5 coupled system for the study of regional climate, chemistry and nitrogen cycle interactions over Africa.

## 1 Introduction

Tropical Africa is a significant source of gas and particles affecting the regional and global atmospheric chemistry and climate. Beside large chemical sources linked to anthropogenic activities (biomass burning, megacities), there is also a significant amount of biogenic emissions which can significantly interact with regional tropospheric composition across various tropical locations (e.g., Aghedo et al., 2007). Nitrogen emissions originating from soil microbial processes are an important component of these emissions (Fudjoe et al., 2023). Indeed, soil microbial processes, such as nitrification and denitrification involve the production of reactive gaseous compounds released to the atmosphere (Delmas et al., 1995; Medinets et al., 2015; Schreiber



et al., 2012). Soil NO (referred as BioNO) emissions dominate the global net nitrogen oxide exchange between ecosystems and the atmosphere (Ludwig et al., 2001) and have been estimated to approximate  $4.7\text{-}26.7\text{ TgN.yr}^{-1}$  above canopy (Davidson and Kinglerlee, 1997; Ganzeveld et al., 2002; Hudman et al., 2012; Jaeglé et al., 2005; Müller, 1992; Steinkamp and Lawrence, 2011; Vinken et al., 2014; Yan et al., 2005; Yienger and Levy, 1995). BioNO emissions play a crucial role in the formation of particles and key atmospheric gaseous compounds, such as  $\text{O}_3$  and  $\text{HNO}_3$  (Liu et al., 2020; Mosier, 2001; Vinken et al., 2014; Williams et al., 2009). Soil microbial processes depend primarily on precipitation and soil moisture (Liu et al., 2009; Li et al., 2022). Over tropical Africa, which shows a marked rainfall seasonality, an accumulation of nitrogen in soils occurs during the dry season, leading to significant pulses of nitrogen emissions at the onset of the rainy season (Austin et al., 2004). Various environmental and physical factors, including wind speed, floristic composition, nitrogen input (from organic and synthetic fertilization and atmospheric deposition), plant cover, soil temperature and moisture, soil pH, and texture, influence BioNO emissions (Delon et al., 2007; Williams et al., 1992).

In tropical Africa, estimating BioNO emissions is however challenging due to a lack of observational data (e.g., Jaeglé et al., 2004; Van Der A et al., 2008). Nevertheless, global and regional modelling approaches, which consider these influences to various degrees, have been proposed to quantify BioNO emissions (e.g., Hudman et al., 2012; Stohl et al., 1996; Stehfest and Bouwman, 2006; Yienger and Levy, 1995; Yan et al., 2005) and ensuing chemical impacts. For instance Williams et al. (2009) used an inventory of biogenic emissions derived from multi-annual simulations of the ORCHIDEE vegetation model (Lathiere et al., 2006) to examine the influence of NO and BVOC emissions from soils and vegetation on Equatorial Africa's tropospheric composition. The global chemistry-transport model simulations revealed that NO emissions from soils in Africa might contribute to 2-45 % of tropospheric ozone production. Delon et al. (2008) used neural network-based parameterization coupled with a mesoscale model to investigate the impact of BioNO emissions on  $\text{NO}_x$  and  $\text{O}_3$  production in the lower Equatorial Africa's troposphere on a specific period (6 August 2006) during the AMMA campaign in the Sahel. Their findings indicate an increase in tropospheric  $\text{O}_3$  and  $\text{NO}_x$  concentrations in the lowest few kilometres of the atmosphere, in response to larger BioNO fluxes, compared to simulations using the prescribed inventory of Yienger and Levy (1995). Steinkamp et al. (2009) used the ECHAM5/MESy atmospheric chemistry model (EMAC) to examine the influence of BioNO on lower tropospheric  $\text{NO}_x$ ,  $\text{O}_3$ , PAN,  $\text{HNO}_3$ , OH, and  $\text{CH}_4$  lifetime ( $\tau_{\text{CH}_4}$ ). Their results revealed that BioNO significantly contributes to  $\text{NO}_x$  levels in numerous regions, especially in the tropics. Moreover, BioNO notably raises OH concentrations, thereby increasing the global troposphere's oxidizing capacity and resulting in an 10% decrease in  $\tau_{\text{CH}_4}$  due to soil NO emissions.

From a modelling point of view, there is a strong interest in integrating interactive BioNO emission in regional climate systems: it can allow for instance to study the impact of present and future climate change and variability, including temperature fluctuations, precipitation patterns, and soil moisture levels, on BioNO emissions. This understanding is crucial for predicting possible future emission trends, potential changes in chemical environment, and developing effective mitigation strategies. Additionally, BioNO emission can affect the formation of ozone and other secondary pollutants, which have implications for air quality and climate forcing and responses, which can be evaluated by means of coupled climate chemistry systems. Furthermore, the regional climate modelling approach allows the study of regional environmental disturbances such as land use and agricultural changes in a flexible way. Finally, Since climatic and land use gradients are particularly important in west and



central Africa, the dynamical downscaling capabilities offered by the regional climate modelling approach are also particularly interesting to capture the regional contrasts in emissions and processes at play. One goal of the present study is to evaluate and extend such a system based on the ICTP RegCM5 model (Giorgi et al., 2023), while estimating and analysing the regional impact of BioNO emissions (from soils and vegetation) on key tropospheric species relevant to the atmospheric nitrogen cycle. The latter plays an important role in the chemistry of the atmosphere as well as the functioning of aquatic and terrestrial ecosystems and agrosystems (McNeill and Unkovich, 2007; Vitousek et al., 1997). This N cycle is significantly disrupted by anthropogenic activities (agriculture, fossil fuel combustion, and biofuels) (Galloway et al., 2008). This issue is particularly concerning in tropical regions like Africa, where rapid population growth and seasonal cycles from natural and anthropogenic sources contribute significantly to changes in N emissions (Adon et al., 2010). We focus on NO<sub>2</sub>, HNO<sub>3</sub>, and O<sub>3</sub> because these species are tightly interconnected and are involved in different environmental and health impacts. NO<sub>2</sub>, a key reactive nitrogen species, contributes to the formation of HNO<sub>3</sub> and O<sub>3</sub>. HNO<sub>3</sub> is formed when NO<sub>2</sub> reacts with other substances in the atmosphere, and is an important contributor of rainfall acidity deposition and nitrogen supply to ecosystems. O<sub>3</sub>, a powerful oxidant, is influenced by the presence of NO<sub>2</sub> and has significant implications in HNO<sub>3</sub> formation. Understanding the concentrations and fluxes of these species is essential for assessing nitrogen management and potential risks in Africa. To a large extent, this work shares scientific goals with, and is carried out as part of the INSA (Integrated Nitrogen Study in Africa; <https://doi.org/10.3030/871944>) and the INDAAF (International Network to study Depositions and Atmospheric chemistry in Africa; <https://indaaf.obs-mip.fr>) projects.

The study is structured as follows: Sections 2 and 3 provide a description of the modelling context and developments, as well as measurement sites and relevant databases used in this study. Section 4 will focus on evaluating model performances in simulating key regional climatic features affecting emissions and tropospheric chemistry. Section 5 will discuss simulated BioNO in more detail. Model results and limitations concerning their impact on key atmospheric chemistry components will be discussed in Section 6.

## 2 Model description

### 2.1 The Regional Climate-chemistry Model RegCM5-CHEM

The present work is based on the latest version of the ICTP RegCM5 discussed in detail in Giorgi et al. (2023). Compared to previous versions, a significant development has been the integration of the MOLOCH non-hydrostatic dynamical core (Davolio et al., 2020) improving model efficiency, notably in view of climate convection-permitting (CP) simulations (e.g., Ban et al., 2021; Coppola et al., 2020; Lucas-Picher et al., 2021; Pichelli et al., 2021; Prein et al., 2015).

This development is also important for atmospheric chemistry, which uses a large number of tracers, by reducing the numerical cost of advection in the context of long-term simulations. As for previous model versions, several options are available for the model physics. In the present study we run successive tests (not discussed further here) to retain a model configuration based on the the RRTM (Rapid Radiative Transfer Model) for shortwave and longwave radiation, the University of Washington turbulence scheme (UW, Bretherton et al., 2004), the Nogherotto et al. (2016) bulk microphysics scheme and the Tiedtke





**Table 1.** Summary of simulations performed for the analysis of regional climate and trace gas in this article.

Name	Period	Spin-up	Description
BASE	Jan 2010 - Feb 2013	Jan-Feb 2010	Base run as release
BIONO	Jan 2010 - Feb 2013	Jan-Feb 2010	Base run + BioNO emissions

90 convection scheme (Tiedtke, 1989). Continental surface processes are treated by the Community Land Model, version 4.5 (CLM4.5, Oleson et al., 2013) which also provides important coupling variables used through the atmospheric chemistry interface, such as surface resistances, soil humidity and temperature. The meteorological boundary condition fields are provided at a six-hourly frequency, from the ERA5 reanalysis (Hersbach et al., 2020). The sea surface temperature data is prescribed by the OI\_WK every week.

95 Atmospheric chemistry processes are based on approaches initially developed in Solmon et al. (2006) and Solmon et al. (2021) for aerosol and Shalaby et al. (2012) and Ciarlo et al. (2021) for gas phases. The chemical reaction solver is here based on the CBM-Z photochemical mechanism module (Shalaby et al., 2012; Zaveri and Peters, 1999). It allows a comprehensive coverage of regionally to globally significant species and reactions involved in photo oxidant chemistry, while keeping a good precision and numerical efficiency. CBM-Z notably includes key prognostic species such as O<sub>3</sub>, NO<sub>x</sub>, CO, VOCs. Aerosol gas  
100 partition is treated here using a thermodynamic equilibrium approach and the ISORROPIA-II scheme (Fountoukis and Nenes, 2007; Nenes et al., 1998) mostly relevant for fine particles heterogeneous processes. Dry deposition processes and fluxes are parameterized according to Zhang et al. (2003), for 31 gas phase species in the model. Key input for Zhang deposition scheme include biophysical and physiological parameters, which are prescribed to the model using pre-defined land use categories and mapping (Dickinson, 1986; Zhang et al., 2002). Some parameters, such as LAI, roughness length, wind, surface temperature,  
105 etc. are provided through the CLM4.5 interface. In the present study, slight modifications have been made in the deposition scheme to account for African regional specificities:

- a. Default ground resistance (R<sub>g</sub>) values for ozone are based on Zhang et al. (2003) were used but for the ocean domain, we adjusted these values by lowering them to obtain more realistic values of dry deposition velocity (e.g., Charusombat et al., 2010; Wu et al., 2011; Zhang et al., 2002) and so surface concentrations over the Ocean.
- 110 b. The friction velocity (u\*) is a crucial parameter for calculating aerodynamic resistance (r<sub>a</sub>). According to Padro et al. (1991), the equation used to calculate r<sub>a</sub> requires that the Richardson number be maintained below 0.21 under stable conditions. This is particularly important in tropical forested areas with weak mean winds, where both u\* and deposition velocity are often lower than those reported in the literature (e.g. Adon et al., 2013; Zhang et al., 2003). To ensure compliance with this criterion, we have set a lower threshold of 0.4 m/s for u\* in forests and 0.1 m/s in savannas, based  
115 on our statistical analysis.

The wet deposition flux is initially parameterized following the approach developed in the MOZART chemistry transport model (Emmons et al., 2010; Horowitz et al., 2003). 26 CBM-Z tracers are considered for wet removal through large-scale and convective precipitation processes. Compared to Shalaby et al. (2012) and Ciarlo et al. (2021), we significantly upgrade the wet deposition parameterizations by developing a new interface which uses directly cloud to rainwater production and precipitation rate terms diagnosed from both the Nogherotto et al. (2016) stratiform and the Tiedtke (1989) convective rain rates.

Anthropogenic and biomass burning emissions are treated through a preprocessing interface designed for the regional interpolation and chemical aggregation of different possible inventories. In this study, the monthly, 0.1 deg resolution emission inventories from the Copernicus Atmosphere Monitoring Service (CAMS, version 6.2) is considered for non-biomass burning emissions (Soulie et al., 2023). For biomass burning, daily emissions from GFED4 (Global Fire Emissions Data, version 4) for 0.25 deg as spatial resolution are considered (Randerson et al., 2018). For both inventories, the lumping of emitted VOC species to effective CBMZ species has been performed following a method similar to Huijnen et al. (2019). The biogenic VOC emissions are calculated on line as part of CLM45 using the embedded MEGAN (Model of Emissions of Gases and Aerosols from Nature; Guenther et al., 2006) scheme. Here only isoprene fluxes are passed to the atmospheric chemistry and transport interfaces (Strada et al., 2023).

Finally, an important development compared to Shalaby et al. (2012) and Ciarlo et al. (2021) concerns the chemical initial and lateral boundary conditions. The standard monthly climatology approach has been replaced here by a new interface using six-hourly CAMS chemical reanalysis (Inness et al., 2019; Wagner et al., 2021), consistent with the ERA5 dynamical forcing. For important chemical and aerosol species, this allows to represent more explicitly the influence and variability of long range chemical transport events possibly affecting the domain through the boundaries.

## 2.2 The BioNO emission parameterization

Interactive BioNO emissions are represented here following the empirical approach developed in Delon et al. (2007) (D2007) based on an Artificial Neural Network (ANN) supervised learning considering several databases. In some regions such as Africa, few in situ measurements of BioNO are available leading to inaccurate estimates of emissions affecting concentrations in the lower troposphere (Jaeglé et al., 2005). The main advantage in using this ANN algorithm is that it can be connected on line and linked to varying environmental parameters of specific regions of interest, and can be used for calculating accurate BioNO emissions whatever the type of soil and/or climate (Delon et al., 2007). For now, this ANN algorithm has been used only in Tropical African climates (Delon et al., 2007, 2012, 2015). The main advantage in using this ANN algorithm is that it's linked to varying environmental parameters of specific regions of interest, and can be used for calculating accurate BioNO emissions whatever the type of soil and/or climate NO emissions are largely influenced by microbial activity, determined by the soil physical properties (porosity, soil texture, soil moisture etc.) governing substrate diffusion and oxygen supply (Skopp et al., 1990). D2007's parameterization includes seven explicative variables, including wind speed, fertilisation rate, surface temperature, sand percentage, soil moisture, soil pH, and deep soil temperature (20-30 cm). Wind speed is used as an indicator of varying atmospheric conditions. Deep soil temperature relates to oxygen diffusion and nitrogen mineralization in the soil (Butterbach-Bahl et al., 2004). The sand percentage impacts water diffusion (Roelle et al., 2001). pH is a crucial factor due



150 to its impact on chemical or biological mechanisms (Serca et al., 1994). It can also influence NO emissions through chemo-  
denitrification process (low pH) or biological activity (higher pH) (e.g., Ormeci et al., 1999; Serca et al., 1994). Finally the  
fertilisation rate is key to reflect the amount of externally introduced nitrogen (Sanhueza et al., 1990). The pH and fertilisation  
rates are prescribed using external databases as inputs: soil pH data are obtained from IGBP-DIS (International Geosphere  
Biosphere Programme-Data and Information System; Igbp-Dis, 1998), and fertilisation rates, including N fertilizer and N  
155 manure, are sourced from Potter et al. (2010). The other variables are integrated on line within the model.

In output, NO emission fluxes are finally calculated at each model time step, through the resulting equations:

$$\text{NOflux}_{\text{norm}} = w_{24} + w_{25} \tanh(S_1) + w_{26} \tanh(S_2) + w_{27} \tanh(S_3) \quad (1)$$

with

$$160 \quad S_1 = w_0 + \sum_{i=1}^7 w_i x_{j,\text{norm}}$$
$$S_2 = w_8 + 15 \sum_{i=8}^{23} w_i x_{j,\text{norm}} \quad (2)$$
$$S_3 = w_{16} + \sum_{i=17}^{23} w_i x_{j,\text{norm}}$$

with  $j = 1 \rightarrow 7$

NOflux<sub>norm</sub> represents the normalised NO flux and the seven inputs mentioned above are represented by  $x_1$  to  $x_7$  (surface  
165 WFPS, surface soil temperature, deep soil temperature, fertilisation rate, sand percentage, pH and wind speed respectively).  
Each input  $x_i$  is associated with a weight  $w_i$ , which represents the strength or influence of that input in determining the final  
NO flux.

### 2.3 Model experiments

To test the ability of RegCM5-CHEM to simulate African climate, BioNO emissions and to evaluate its effect on atmospheric  
170 chemistry, we conducted two different simulations which are listed in Table 1. The simulations cover the period from January  
2010 to February 2013, which includes a variety of climatic conditions and seasonal variations. The first two months are used  
as spin-up time for both experiments and are not considered in the analysis of the results.

1. BASE run: BASE run: With biomass burning and anthropogenic emissions, without BioNO emissions.
2. BIONO run: With biomass burning, anthropogenic emissions and BioNO emissions.

175 The model is 30 km \* 30 km in longitude and latitude, with 35 vertical levels from the surface to 3.6 hPa. The corresponding  
model time step is 210 s.



### 3 Data and study sites

#### 3.1 Study sites and ground-based observation of pollutants

O<sub>3</sub>, NO<sub>2</sub> and HNO<sub>3</sub> concentrations are measured in the framework of the INDAAF long-term monitoring project. INDAAF, part of the Aerosol Cloud and Trace gases Infrastructure (ACTRIS-Fr), represents a long term monitoring service to study evolution of atmospheric chemical composition and deposition in Africa. Gaseous concentrations are monthly measured on different sites in West and Central Africa and data are distributed at <https://indaaf.obs-mip.fr>. Datasets are referenced for each sites using DOIs (<https://doi.org/10.25326/608>; <https://doi.org/10.25326/604>; <https://doi.org/10.25326/605>; <https://doi.org/10.25326/275>; <https://doi.org/10.25326/607>; <https://doi.org/10.25326/603>). We use observations from six sites representative of the main african ecosystems (Figure 1, Table 2): Dry savannas (Banizoumbou, Katibougou), Wet savannas (Lamto, Djougou) and equatorial Forests (Bomassa, Zoétélé). Gas monitoring at Banizoumbou, Katibougou, Lamto, Bomassa and Zoétélé started in 1998, with the Djougou site joining in 2005. Atmospheric gas concentrations (NO<sub>2</sub>, HNO<sub>3</sub>, O<sub>3</sub>) are performed using passive sampling techniques based on the methodology outlined by Ferm et al. (1994). Developed by the Laboratory of Aerologie (LAERO) in Toulouse within the framework of the INDAAF project, these passive samplers underwent rigorous testing across various tropical and subtropical regions (Adon et al., 2010; Carmichael et al., 2003; Ferm and Rodhe, 1997). Continuous measurements are ongoing at all INDAAF sites, and data are available for the entire period of our study from January 2010 to February 2013. Although there are some missing data for certain months in specific ecosystems, the overall dataset provides a comprehensive view for the analysis.

**Table 2.** Site coordinates and location information. Dry savannas (ws: June–September, ds: October–May), Wet savannas (ws: April–October, ds: November–March), Forests (ws: March–November, ds: December–February). ws: wet season, ds: dry season.

Ecosystems	Station	Latitude, Longitude	Type of soil and/or vegetation	Climate	Country
Dry savannas	Banizoumbou	13°18' N, 02°22' E	91.2% Sandy soils, Tiger bush – fallow bush	Sahelian	Niger
	Katibougou	12°56' N, 07°32' W	Sandy soils, Deciduous shrubs	Sudano-Sahelian	Mali
Wet savannas	Djougou	09°39' N, 01°44' E	Ferralitic and ferruginous soil, Mosaic of dry forests and savannah	Sudano-Guinean	Benin
	Lamto	06°13' N, 05°02' W	Ferruginous soils, Grass, shrub and tree stratum	Guinean	Côte d'Ivoire
Forests	Bomassa	02°12' N, 16°20' E	Dense evergreen forest	Equatorial	Republic of Congo
	Zoétélé	03°10' N, 11°49' E	Dense evergreen forest	Equatorial	Cameroon

Detailed description and accuracy of INDAAF passive samplers are given in previous African studies, encompassing rural and urban sites (Adon et al., 2010; Bahino et al., 2018; Carmichael et al., 2003; Ferm and Rodhe, 1997; Galy-Lacaux et al., 2009;

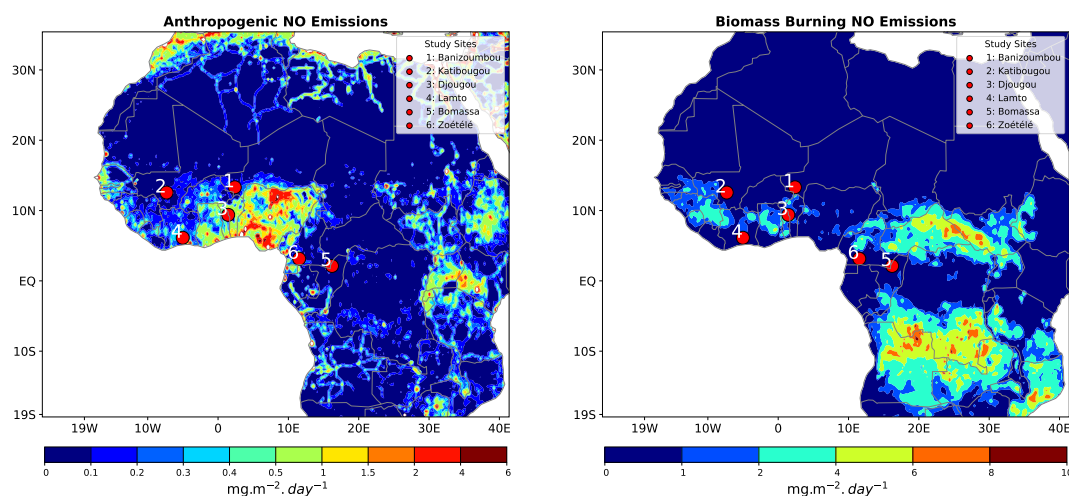


**Figure 1.** Annual anthropogenic and biomass burning NO emission (averaged over 2010-2013) and INDAAF measurement sites localization: Banizoumbou, Katibougou, Djougou, Lamto, Bomassa and Zoétélé.

Galy-Lacaux and Modi, 1998; Ossohou et al., 2019, 2023). Monthly mean concentrations (used here as reference) are derived from the duplicates' means. Upon completion of the exposure period, all samplers, including field blanks, undergo laboratory analysis using ionic chromatography. The LAERO bi-annually participated in the WMO-GAW (World Meteorological Organization - Global Atmosphere Watch) quality assurance program since 1996, evaluating the precision of ionic chromatography measurements for trace compounds twice yearly. Results, accessible under reference 700106 at <http://qasac-americas.org/>, consistently demonstrate analytical precision of 5% or better for all ions. Additionally, the measurement accuracy of passive samplers, assessed through covariance with duplicates, was estimated at 9.8% for NO<sub>2</sub>, 20% for HNO<sub>3</sub>, and 10% for O<sub>3</sub> (Adon et al., 2010). Detection limits, determined using the exposure period and field blanks for the studied duration, are reported as 0.2 ± 0.1 ppb for NO<sub>2</sub>, 0.07 ± 0.03 ppb for HNO<sub>3</sub>, and 0.1 ± 0.1 ppb for O<sub>3</sub>.

### 205 3.2 Climatic and chemical evaluation datasets

For further model evaluation, we use a variety of sources, including data from meteorological stations and satellites, as well as reanalysis products. Table 3 summarises information about all variables used from each database. Precipitation data are obtained from the Tropical Rainfall Measuring Mission 3B42-version 7 (TRMM; Huffman et al., 2007). Temperature data are sourced from the Climatic Research Unit version TS4.03 (CRU; Harris et al., 2020). For circulation dynamics, we use data derived from the European Environment Agency version 5 (ERA5; Hersbach et al., 2020). CRU data is exclusively based on



in situ observations, while TRMM data originates from satellite observations. As mentioned above, ERA5 reanalysis data is derived from a combination of in situ measurements and satellite observations assimilated in a Numerical Weather Prediction model simulation. By using different sources of observational data (in situ and satellite) as well as reanalysis estimates, for precipitation (Pr), wind field (U,V, and W), and 2 m surface temperature (T), we account for associated uncertainties, particularly in West Africa.

**Table 3.** Summary of validation data for physical parameters.

	TRMM	CRU	ERA5
Variables	Pr	T	T, U, V et W
Spatial resolution	0,25°	0,5°	0.25°
Spatial coverage	Ocean/Land	Land	Ocean/Land
Period	1997-2020 (6H)	1901-2018 (mensual)	1940-present (6H)

For the chemical evaluation, the model outputs were compared with the INDAAF in-situ measurement database. To complement this local evaluation we also compare the model to CAMS chemical reanalysis (Inness et al., 2019; Wagner et al., 2021), and to outputs from the state of the art chemistry transport model GEOS-Chem (Goddard Earth Observing System-Chemistry; <https://doi.org/10.5281/zenodo.3974569>), and ground-level NO<sub>2</sub> concentrations derived from OMI and TROPOMI satellite NO<sub>2</sub> observations (Cooper et al., 2022).

GEOS-Chem is a global 3D Chemical Transport Model (CTM) driven by assimilated meteorological observations from NASA's Goddard Earth Observing System (GEOS). It addresses atmospheric composition issues across local to global scales. CAMS (Copernicus Atmosphere Monitoring Service) provides chemical reanalysis data by assimilating diverse observational sources, including satellite and in-situ measurements, which improves the accuracy of the simulated chemical fields. The ground-level NO<sub>2</sub> concentrations were derived from OMI and TROPOMI satellite observations (Cooper et al., 2022). Initially determined using OMI, these NO<sub>2</sub> column densities were downscaled using TROPOMI, then converted to surface concentrations with the GEOS-Chem model, constrained by ground monitoring data (Cooper et al., 2020, 2022). Both CAMS and GEOS-Chem are subject to their own model uncertainties, however with an added observational constraint in the case of CAMS reanalysis. TROPOMI-derived NO<sub>2</sub> data also carries uncertainties, particularly in the conversion from column densities to surface concentrations, which may introduce discrepancies. These include potential errors in satellite retrievals and air mass factor calculations.



#### 4 Regional Climate validation

The simulation of African climate by the model is evaluated in terms of seasonal and daily mean for the 3 simulated years. An exhaustive analysis of climate simulations is out of the scope of this paper. We report here model performance in terms of temperature, precipitation and monsoon circulation, which are key features of the African climate, strongly impacting atmospheric chemistry.

Figure 2 compares the ERA5 reanalysis to simulated mean wind at 850 hPa i.e. in the monsoon layer. Overall the model manages to reproduce the main features of the monsoon circulation with a mean characteristic southwesterly flow up to about 17°N, and Harmattan-like circulation over northern Africa. However RegCM5 tends to underestimate the intensity of the mean monsoon flow from the Gulf of Guinea to the Sahel. The monsoon front and the Saharan Heat Low (SHL) are also reasonably captured by the model, although the SHL amplitude is somehow underestimated (Figure 2). This could explain or contribute to the weaker Monsoon flux and the sahelian precipitation underestimation discussed further (Figure 3-c) following the connections described in Peyrillé et al. (2007), Lavaysse et al. (2009), Chauvin et al. (2010), Lavaysse et al. (2010) and Evan et al. (2015). Outside of the monsoon domain, the central equatorial Africa wind minimum is consistently captured.

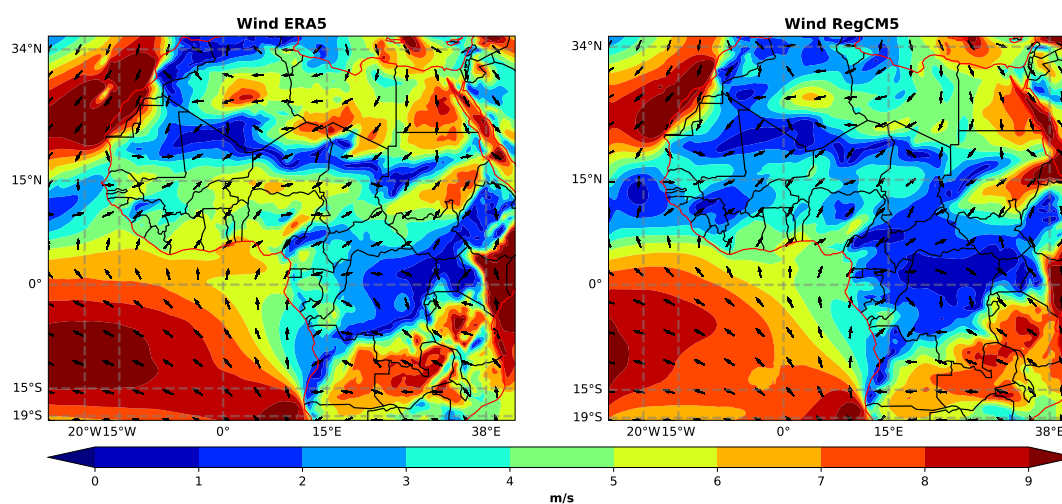


**Figure 2.** JJA Monsoon wind speed at 875 hPa for ERA5 reanalysis and RegCM simulation.

RegCM5 captures the patterns and spatial gradients of the 2 m surface temperature from hot Sahara regions to colder tropical forests, but with a cold bias over the northern Sahel/Southern Sahara ( range -5 to -1 °C) during the monsoon season





(JJA) (Figure 3-f). Attributing surface temperature bias to specific causes is uneasy due to temperature surface-atmosphere interactions and feedbacks (Sylla et al., 2012; Tadross et al., 2006). For Sahelian and Sahara regions RegCM shows a negative bias which is likely linked to a bias in surface radiative budget, depending on simulated surface SW and LW net radiation related to surface radiative parameters, possible excessive high level cloudiness (e.g., Sylla et al., 2012; Zittis et al., 2016) or/and aerosol for instance (e.g., Lavaysse et al., 2011; Wang et al., 2015). In the heat low region, this cold bias is likely consistent with weaker monsoon flux and sahelian precipitation. In the equatorial region the temperature bias could be linked, on the contrary, to excessive cooling induced by overestimated precipitations. Sylla et al. (2012) showed that cold bias in surface temperature is generally consistent with positive rainfall bias. Locally the surface temperature overestimation over coastal central Africa has also been noticed by Mbienda et al. (2023). This bias in Central Africa might stem from an inadequate modelling of the low-level cloud cover that is typical of this area (Philippon et al., 2019). For precipitation, simulated values vary from 0 to more than 13 mm/day over the study domain, with a consistent spatial/seasonal (Figure 3a-b) pattern of precipitation compared to TRMM observation. In general, the most predominant biases in our simulation are an underestimation in Sahel and Central Africa and an overestimation closer to equatorial regions (about from -5 to -0.5 in Sahel/Central Africa and 1 to 5 mm/day in Cameroon Highlands). We also observe the rain belt over the Sahelian region, associated with the InterTropical Convergence Zone (ITCZ) stretching from the mountains of Darfur in East Africa to the Guinea Highlands and downstream into the Atlantic. In some subregions, observation data sets do not fully agree. For instance, in comparison to GPCP data, which is consistent with gauge-based precipitation datasets in Africa (Sylla et al., 2013b), TRMM data shows weaker precipitations over East Africa and the Guinea Highlands, and over the Cameroon Highlands (Nikulin\* et al., 2011; Nikulin et al., 2012). This variability amongst observations should be kept in mind while evaluating the model results. As outlined in many studies, the model precipitation is extremely sensitive to the choice of parameter combinations used in the physics configurations, such as convection, land surface scheme, boundary layer, etc. The number of parameter combinations is large and model optimization is a complex and often time-consuming issue (e.g., KhayatianYazdi et al., 2021). With the present set up, the main precipitation and temperature biases remain reasonable, especially considering the range of bias shown by state of the art CMIP6 (Coupled Model Intercomparison Project phase 6) Global Climate Models and CORDEX (COrdinated Regional Downscaling EXperiments) RCMs for the African climate simulations (e.g., Buccignani et al., 2018; Zittis et al., 2016). For the west African region, Figure 4 shows a time-latitude Hovmoeller diagram of precipitation zonally averaged between 10°W and 10°E for the RegCM5 model and TRMM observational data. Both in model and observations, the three characteristic phases of the African monsoon (Hourdin et al., 2010; Koné et al., 2022; Sultan et al., 2003) are highlighted. For TRMM, the onset of the rainy season occurs in mid-April and extends until mid-June, as evidenced by the core of the rainfall band along the Guinea coast between approximately 4° and 7°N, while the simulations show a delayed onset from mid-May to June with lower intensity rainfall. In TRMM observations, the monsoon phase itself is characterised by a shift of the rainfall maximum band between July and September reaching 15°N. For this phase, the simulations show a consistent northward precipitation shift, but the maximum does not penetrate as far north as in the observation, in relation with the Sahelian precipitation underestimation pointed out earlier. The monsoon withdrawal is observed with precipitation gradually shifting towards the coast. The late season precipitation rainfall is more intense in our simulations compared to TRMM. Again these characteristic seasonal patterns are

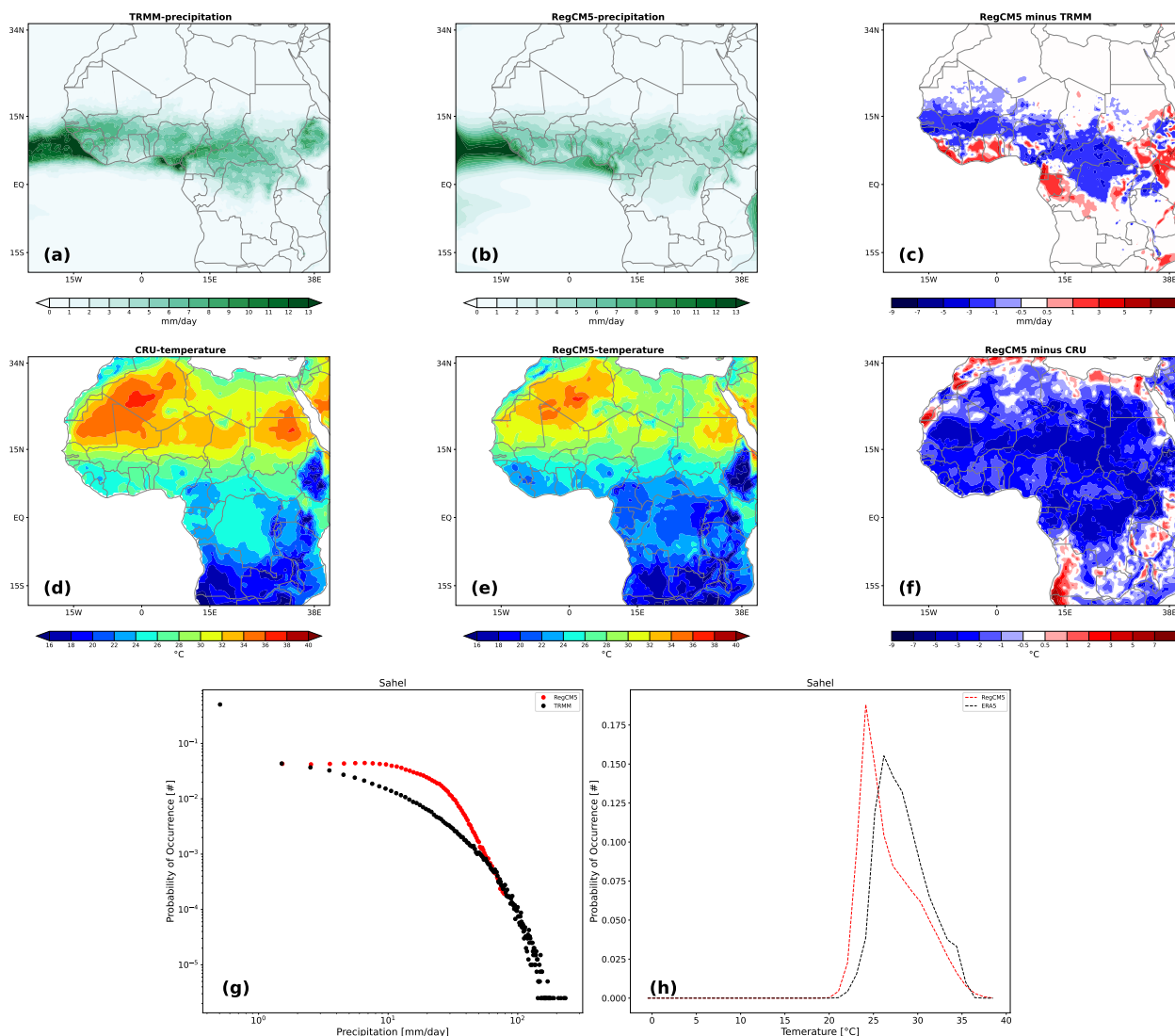


**Figure 3.** Summer (JJA) means Precipitation and Surface Temperature Biases (TRMM and CRU vs. RegCM5), and Frequency of Daily Temperature and Precipitation Events (ERA5, TRMM, and RegCM5). Units: Precipitation in mm/day, Temperature in °C.

rather satisfactorily captured by the model in reference to state of the art climate models.

Beyond seasonal means, simulated daily temperature and precipitation intensity variability are also analysed using Probability Density Functions (PDFs) (Giorgi et al., 2023) and compared to ERA5 and TRMM respectively. These are presented here, for 285 June-July-August of the study period, for the model and the observations in Figures 3-g and 3-h on the Sahel region, which has a particular meteorological regime for precipitation and where the relevant impact of BioNO occurs: Sahel (10°W-10°E; 10°N-16°N).



For the daily temperature PDFs (Figure 3-h), the model simulation captures the observed distribution, although over the region, RegCM5 peaks are slightly shifted compared to the ERA5 data. Overall we observe that simulated values between 20 and 30 °C appear with a high frequency of occurrence (more than 18 %) while we have less than 15 % for temperatures above 30°C. However, ERA5 presents the higher frequency of occurrence for high temperatures (25-35 °C) over the region with 2-16 %, against 1-13 % for simulated values. This can also be linked to the underestimation shown by RegCM5 compared to the observation (Figure 3-f).

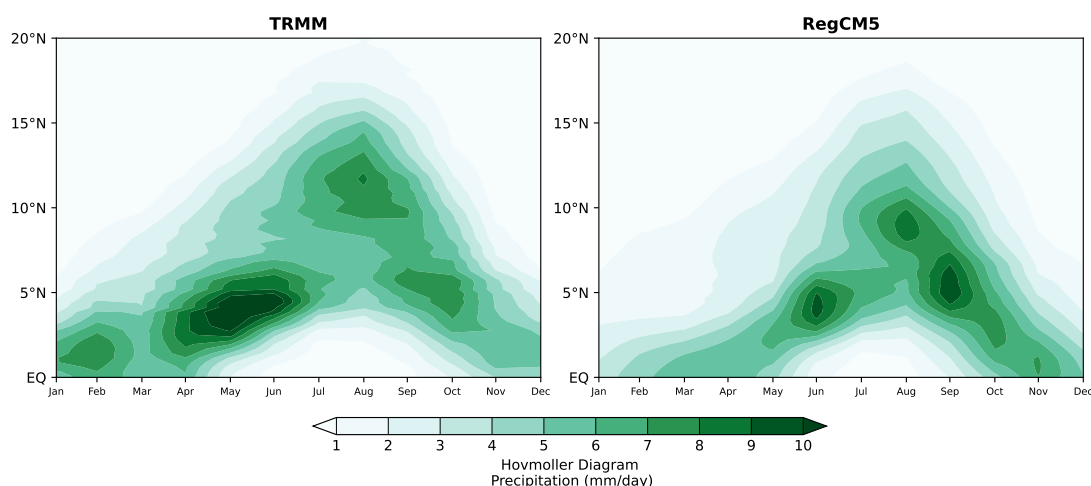


**Figure 4.** JJA Hovmoller diagram of monthly precipitation ( $\text{mm}\cdot\text{day}^{-1}$ ) averaged between longitudes  $10^{\circ}\text{W}$  and  $10^{\circ}\text{E}$  of the study period.

The corresponding precipitation PDFs are intercompared in Figure 3-g. Overall, RegCM5 is close to TRMM in low (less than 10 mm/day) and high (more than 100 mm/day) precipitation intensities. Over the domain, RegCM5 is characterised by higher frequencies of mid precipitation intensities (between 10 and 60 mm/day) than TRMM. For high precipitation intensities (more than 70 mm/day), simulated precipitation intensity frequencies remain lower than the observed ones, consistently with the mean precipitation bias shown in Figure 4 (cold bias for sahel region).

The simulation quality is considered at this stage good enough for supporting further analysis focusing on atmospheric chemistry.

## 5 BioNO fluxes

Since soil moisture is an important driver of microbial activity and BioNO emissions (Skopp et al., 1990), we evaluated simulated soil moisture compared to the Famine Early Warning Systems Network Land Data Assimilation System FLDAS



(McNally et al., 2017, 2018) (Figure 5). As shown in the figure, JJA soil moisture is larger in subregions dominated by dense  
305 vegetation (Forests regions:  $-7^{\circ}\text{N}$ - $4^{\circ}\text{N}$ ) and where precipitation events are more intense. Despite the overall slight underes-  
timation of simulated soil moisture compared to FLDAS observed data, especially in Saharan regions, RegCM captures the  
spatial distribution of soil moisture both in DJF and JJA. FLDAS integrates various observational datasets and uses advanced  
modelling techniques to provide soil moisture data, but its accuracy in arid regions like the Sahara can be challenging due  
to sparse in-situ data and the extreme dryness of the environment. Soil moisture data in such regions are often derived from  
310 remote sensing sources like microwave satellites, which can struggle with accuracy in arid zones where ground measurements  
are extremely rare (Rao et al., 2022). The BioNO emission spatial distribution reflects the influence of the different explicative  
variables considered in the D2007 ANN. Overall, in both seasons, weak BioNO emissions in Saharan regions (above  $16^{\circ}\text{N}$ ),  
are associated with low N content, no N input, low soil moisture and a high sand percentage. A high sand percentage leads to  
increased evaporation and drainage rates (Delon et al., 2008), which prevents the soil from retaining enough water to support  
315 the microbial processes responsible for NO emissions. Between  $8$  and  $16^{\circ}\text{N}$  (Sahel), higher BioNO emission spots result in a  
combination of large soil moisture, latitudinal distribution of soil pH (less high), and significant nitrogen input (shown in Potter  
et al., 2010). The seasonal variability of Sahelian emission hot spots is mostly driven by soil humidity as illustrated on Figure 5.  
There is also a significant canopy inhibition factor in the region of large LAI which for example reduces forest emission to the  
atmosphere. As outlined in Delon et al. (2008), the Artificial Neural Network (ANN) algorithm used in this study tends to be  
320 more suitable for the Sahel region because it is primarily trained on data from semi-arid regions and temperate zones, making  
it more uncertain in forested regions where the environmental conditions and soil characteristics differ significantly. In forested  
areas, factors such as dense canopy cover (affecting soil temperature and moisture), higher organic matter content (affecting  
nitrogen cycling dynamics), and different microbial communities influence soil processes and NO emissions (Davidson et al.,  
2000; Pilegaard, 2013) differently compared to semi-arid and temperate zones. This discrepancy highlights the need for further  
325 region-specific training data to improve the model's accuracy in diverse ecosystems.

The limited flux measurements for BioNO emissions in Africa make a systematic evaluation of the model challenging. In this  
study, simulated BioNO range from  $0.02$  to  $7 \text{ mg}\cdot\text{m}^{-2}\cdot\text{day}^{-1}$ , i.e from  $0.1$  to  $37.52 \text{ ngN}\cdot\text{m}^{-2}\cdot\text{s}^{-1}$  as seasonal averaged flux  
over the domain. This is within the range given by Delon et al. (2008) (from  $0.43$  to  $6.52 \text{ mg}\cdot\text{m}^{-2}\cdot\text{day}^{-1}$ ) and Davidson and  
Kingerlee (1997) (from  $0.5$  to  $28 \text{ ngN m}^{-2}\cdot\text{s}^{-1}$ ). The simulated BioNO are also rather consistent with the measured fluxes  
330 from the flight B227 observed data of the British Aerospace 146 (BAe-146) under the Facility for Airborne Atmospheric  
Measurements (FAAM) program:  $0.8$  to  $35 \text{ ngN m}^{-2}\cdot\text{s}^{-1}$ , but remain greater than the Ganzeveld et al. (2002) estimation :  $2.32$   
to  $11.6 \text{ ng N}\cdot\text{m}^{-2}\cdot\text{s}^{-1}$ , for the Sahel region. Our simulated BioNO are in better agreement with NO fluxes from soil measured  
during the DACCWA field campaign West Africa) in June and July 2016, which ranged from  $0$  to  $48.39 \text{ ngN m}^{-2}\cdot\text{s}^{-1}$  (Pacifico  
et al., 2019). Feig et al. (2008) also obtained NO flux fields from  $4.7$  to  $27.01 \text{ ngN m}^{-2} \text{ s}^{-1}$ , but for South Africa. The summary  
335 of all these estimates can be found in table 4 and additional measurements of BioNO emissions from wet African savannas can  
be found in table 7 of Delon et al. (2012).

As for the total amount of nitrogen emitted from BioNO on the whole domain, simulated values range from  $0.01$  to  $4.4$   
 $\text{TgN}\cdot\text{month}^{-1}$ . If we downscale for the Sahel region ( $10\text{W}$   $10\text{E}$ ,  $10\text{N}$   $20\text{N}$ , and area of  $2.3 \cdot 10^6 \text{ km}^2$ ) as done in Stewart et al.

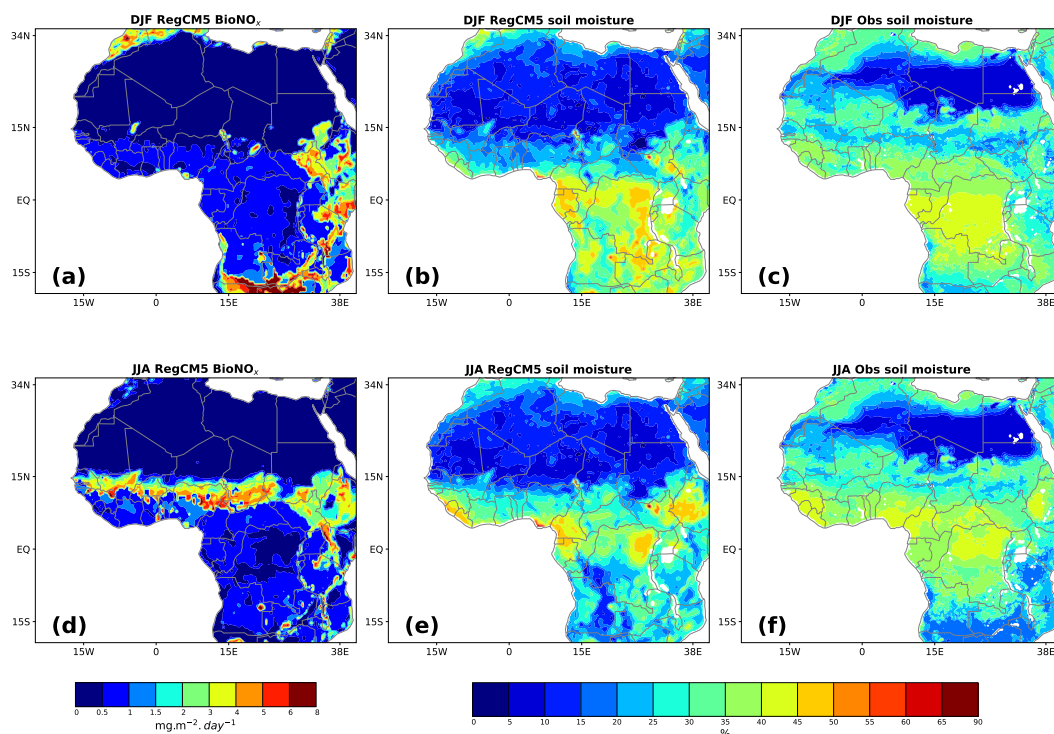


**Figure 5.** Simulated BioNO emissions (in  $\text{mg.m}^{-2}.\text{day}^{-1}$ ) and Soil Moisture Comparison for DJF and JJA Seasons: Analysis Using FLDAS Noah Land Surface Model L4 for 10-40 cm Soil Depth (in %).

(2008), the simulated emissions amount ranged from  $0.0006$  to  $0.23 \text{ TgN. month}^{-1}$ . This value is consistent with Stewart et al. (2008) estimates of  $0.03$  to  $0.3 \text{ TgN}$  for 2 months (July and August) and Yan et al. (2005) estimates of  $1.373 \text{ TgN.yr}^{-1}$  for the entire Africa. Delon et al. (2010) also showed an annual estimate of  $0.35 \text{ TgN. yr}^{-1}$  over the Sahel region. Vinken et al. (2014) showed on the same domain (Sahel) an annual total of  $0.52 \text{ TgN. yr}^{-1}$  with a top-down soil  $\text{NO}_x$  emission inventory for 2005 based on retrieved tropospheric  $\text{NO}_2$  column from the Ozone Monitoring Instrument (OMI).

Our total estimated amount is consistent with Williams et al. (2009) estimated BioNO in the same Sahel region ( $0.575 \text{ TgN.yr}^{-1}$ ) which is based on biogenic emission inventories provided by Granier et al. (2000) and Lathiere et al. (2006). It's worth



**Table 4.** Summary of some BioNO emissions estimates from literature

Regionc/Biomes	Range of fluxes (ngN.m <sup>-2</sup> .s <sup>-1</sup> )	Period	Citation
Sahel	2.32 - 35.29	August 2006	Delon et al. (2008)
Sahel	2.32 - 11.6	-	Ganzeveld et al. (2002)
Niger	0.8 - 35	August 2006	Flight B227 ( <a href="https://www.faam.ac.uk">https://www.faam.ac.uk</a> )
West Africa	0 - 48.39	June-July 2016	Pacifico et al. (2019))
Semi-arid savanna (South Africa)	4.7 - 27.01	June 2003-October 2005	Feig et al. (2008)
Semi arid sahelian rangeland (Dahra, Sénégal)	2 - 10	July 2012, July 2013, November 2013	Delon et al. (2017)

noting that our estimated emission fluxes, particularly in the Sahel region, are higher than those reported by Simpson and Darras (2021) using the EMEP MSC-W model (Meteorological Synthesising Centre – West of the European Monitoring and Evaluation Programme), part of the Copernicus Atmosphere Monitoring Service (CAMS) project. Their estimates ranged from 0 to 3.5 mg m<sup>-2</sup> day<sup>-1</sup> over the study period and region. The ANN algorithm incorporates, here additional surface controlling parameters, which may explain the higher emission fluxes obtained in our study.

## 6 RegCM simulations and impact of BioNO emissions

### 6.1 Regional and local nitrogen

#### 6.1.1 NO<sub>2</sub> concentration

We first analyse the simulated seasonal surface nitrogen (NO<sub>2</sub> and HNO<sub>3</sub>) concentrations for the BASE run over the domain, in comparison with the CAMS reanalysis (Inness et al., 2019; Wagner et al., 2021) and outputs coming from Geos-Chem model. Simulated NO<sub>2</sub> concentration's variability over the domain is primarily driven by regional biomass burning emissions. We thus note consistent spatial and seasonal patterns between RegCM simulations, CAMS and the Geos-Chem (Figure 6) reflecting the broad spatial agreement between the different biomass burning emission inventories considered in these models. However sub-regional details, for instance over west Africa, can be clearly distinguished in higher resolution models against coarse Geos-Chem. Compared to the CAMS reanalysis and to Geos-Chem, the RegCM-BASE shows lower surface NO<sub>2</sub> concentrations (about 0.7-0.9 ppb below), especially in the Sahel regions during the summer. In the Biomass burning regions, these differences are less visible. The biomass burning regions, which are primarily located in the central (in DJF) and southern (in JJA) parts of Africa, are areas where extensive burning occurs.





365 This difference in NO<sub>2</sub> concentration magnitude can be attributed to possible differences in NO emissions (biomass burning, anthropogenic inventories and BioNO) as BioNO emissions were not accounted for in the BASE simulation (cf section 2.3). Differences in biomass burning injection heights and nitrogen fluxes considered in RegCM versus CAMS and Geos-Chem could also explain differences in surface concentrations. The introduction of BioNO fills this gap to some extent, by increasing surface NO<sub>2</sub> concentration, bringing it closer to, or even exceeding CAMS values (Figure 6b,f). This is especially apparent  
370 in transitional ecosystems such as savannas and grasslands. To assess the potential importance and to quantify the impact of BioNO emission on lower troposphere NO<sub>2</sub>, Figure 9 shows the difference between the BioNO and the BASE simulations previously described. The plots are shown on a vertical cross section averaged between -10 and 10 °E, from 4 to 21 °N.

When comparing RegCM5 results to the TROPOMI-derived annual mean ground-level NO<sub>2</sub> concentrations (7) over the period  
375 2010-2013, it becomes apparent that the model generally performs well in capturing the spatial patterns of NO<sub>2</sub> across the region, particularly in transitional ecosystems where the impact of BioNO is significant. However, the model tends to overestimate NO<sub>2</sub> concentrations compared to the TROPOMI observations. This overestimation could be attributed to several factors, including the representation of biogenic and biomass burning emissions in the model, as well as the inherent uncertainties in the satellite-derived data. As detailed by Cooper et al. (2022), uncertainties in the conversion of satellite-observed NO<sub>2</sub>  
380 column densities into surface concentrations can lead to discrepancies. These uncertainties include potential errors of around 10% in the retrieval of slant columns from satellite radiances and errors ranging from 23 to 37% in the calculation of air mass factors. Moreover, the use of ground-monitor data to constrain the model may introduce biases, particularly in regions with sparse monitoring data. These factors suggest that while RegCM provides a reasonable representation of NO<sub>2</sub> distribution, the apparent overestimation relative to TROPOMI may also be partly due to these uncertainties in the satellite-model processed  
385 data.

In this study, we also compare the RegCM5 simulations to the OMI/Aura-derived tropospheric NO<sub>2</sub> columns (<https://doi.org/10.5067/Aura/OMI/DATA3007>) over the period 2010-2013 (Figure 8). The satellite data come from the Level-3 daily global gridded 0.25x0.25 degree OMI NO<sub>2</sub> product (OMNO2d), which provides total and tropospheric NO<sub>2</sub> columns for all atmospheric conditions and is cloud-screened for sky conditions where cloud cover is less than 30%. With its high spatial  
390 resolution (0.25° x 0.25°), this dataset is well-suited for studying large-scale NO<sub>2</sub> distributions in the troposphere. It becomes clear that the model captures the general spatial distribution of NO<sub>2</sub> across the region. Both the model and the satellite data show high concentrations of NO<sub>2</sub> in areas such as Sahel and forests regions, where biomass burning plays a significant role. The spatial correlation analysis shows moderate agreement between the RegCM5 simulations and the satellite-derived data. Specifically, the Pearson Correlation Coefficient (PCC) indicates a correlation of 0.32 when excluding BioNO emissions (No  
395 BioNO) and a correlation of 0.22 when BioNO emissions are included in the simulation. This suggests that the addition of BioNO emissions reduces the overall correlation with the OMI observations. One potential explanation for this reduction could be related to the fact that OMI measures the entire tropospheric column, which may not fully capture diffuse biogenic emissions or localized sources (e.g., Ossouhou et al., 2019) that contribute to near-surface concentrations represented in the model. Despite





some discrepancies in specific regions, the spatial correlation suggests a reasonable alignment of NO<sub>2</sub> patterns between the  
400 model and the satellite observations, particularly in regions where biomass burning and other large-scale processes dominate.

The effect of BioNO emissions from the ANN algorithm at the regional scale, leads to an overall increase in NO<sub>2</sub> seasonal  
mean concentrations ranging from 0 to 2-4 ppb. This increase also extends to the lower troposphere, as illustrated in Figure  
9. The maximum increase occurs over the Sahel region (especially 10-21°N) and can reach up to 3 ppb in JJA, consistently  
with increased BioNO fluxes in this region. We can note a general positive correlation between the BioNO fluxes emissions  
405 (Figure 5a,d) and the difference [BIONO - BASE] simulations at the surface level (Figure 16a,d). This increase in surface  
NO<sub>2</sub> concentrations over the domain is consistent with Delon et al. (2008) results who report that a local BioNO induced NO<sub>2</sub>  
increase by up to 0.9 ppb at 4°E and between 7°N-21°N for August. Based on global simulations, Steinkamp et al. (2009)  
found an increase in global NO<sub>x</sub> mean mixing ratio in the lower troposphere reaching 7 and 17 % for DJF and JJA respectively.  
To further examine the simulated NO<sub>2</sub> concentrations, we compare the results with monthly averaged surface concentrations  
410 from the INDAAF stations. Simulated outputs at the lower model level (around 40 m above the ground level) are interpo-  
lated to the site locations for the simulated period. BIONO and BASE biases (based on the 3-years monthly-averaged mass  
concentration) (Table 5) and correlation with observations (Figure 11) were calculated for the pollutant at the corresponding  
stations.

Figures 10 and 11 show that the BASE model experiment tends to generally underestimate the NO<sub>2</sub> concentrations except for  
415 december-january in wet savannas (Lamto, Djougou). This is also generally the case for the CAMS reanalysis (Figure 10).  
RegCM5-BASE NO<sub>2</sub> concentrations tend to be underestimated especially over dry savannas (Banizoumbou, Katibougou) in  
the wet season, where the maximum negative bias recorded could reach  $\approx -4$  ppb in June and October at the Banizoumbou  
site. Mostapha et al. (2019) used the RegCM4-CHEM and also showed that the model mostly underestimates, compared to  
the Greater Cairo observation (Egypt), the monthly averages of NO<sub>2</sub> concentrations at four representative sites with maximal  
420 underestimation in April. Taking into account BioNO emissions has a very significant impact on reducing the dry savanna's  
wet season bias, as illustrated on figures 10 and 11. Figure 10 suggests that this reduction can bring for instance the model  
maximum negative bias to  $\approx -3.94$  ppb when BioNO are accounted for, vs -4.62 ppb in the BASE run, in July at Banizoumbou.  
We can however notice on figure 9 that the model (BIONO run) tends to produce maximum concentration in the middle of the  
rainy season, while the observations tend to show that maximum NO<sub>2</sub> concentrations occur at the beginning and end of the wet  
425 season (in a sort of bi-modal pattern). This could be due to nitrogen pool limitation not accounted for by the ANN approach  
which reacts only to environmental conditions. Indeed, soil N content in the Sahel shows a maximum at the end of the rain  
season when senescent herbaceous biomass begins to decompose, leading to increased BioNO fluxes (not represented by the  
model). The temporal distribution of rain events might be also at play here, with peak of emissions occurring preferentially  
for rainfall events consecutive to a dry period, which are more likely at the beginning and end of the rainy season (Gasche and  
430 Pape, 1999; Hickman et al., 2018; Johansson et al., 1988; Jaeglé et al., 2005; Yienger and Levy, 1995).

For wet savannas, the model and measurements are rather consistent in the BASE run. During the dry season, positive  
biases are present in the BASE run for wet savannas (unlike dry savannas), ranging between 0.2 and 1.6 ppb. The highest NO<sub>2</sub>  
surface concentrations in the dry season are linked to biomass burning emissions (Oppenheimer et al., 2004; Van Marle et al.,



2017). Moreover, Ossohou et al. (2019) suggested that NO<sub>2</sub> concentrations in the dry season could be mainly attributed to the intensity of biomass burning sources in all the six sites except Banizoumbou and Katibougou. This context helps to explain the observed positive biases, which might be enhanced by the addition of BioNO emissions. While BioNO emissions lead to a small improvement in simulations, especially for the Lamto station during both wet and dry seasons, they tend to worsen these biases. For instance, the maximum positive bias is increased by 1.2 ppb in January at the Djougou site (79.9% increase in bias). The BioNO emissions are possibly overestimated due to larger, and excessive, response of the ANN to soil moisture in wet savanna compared to dry savanna in both seasons (5), which can also combine with a smaller canopy reduction factor when compared to forested regions.

**Table 5.** BASE and BIONO Biases (ppb) for NO<sub>2</sub>. The Reduced/Increased (Red/Inc) biases given by BIONO run is in %. Ba: Banizoumbou, Ka: Katibougou, La: Lamto, Dj: Djougou, Bo: Bomassa, Zoétélé: Zo

		Month												
		Jan	Feb	Mar	Apr	May	Jun	Jul	Aug	Sep	Oct	Nov	Dec	
Dry Savannas	Ba	BASE <sup>a</sup>	-0.47	-0.67	-0.48	-2.01	-2.86	-4.62	-3.28	-2.04	-2.15	-4.97	-1.92	-0.72
		BIONO <sup>b</sup>	-0.43	-0.63	-0.47	-1.84	-2.62	-3.94	-0.48	3.53	0.97	-4.26	-1.85	-0.68
		Red/Inc <sup>c</sup>	-7.42	-6.45	-2.38	-8.38	-8.39	-14.65	-85.46	73.17	-54.86	-14.27	-3.48	-5.57
	Ka	BASE	-0.64	-0.41	-1.54	-2.4	-2.42	-3.02	-1.3	-1.52	-1.13	-1.47	-2.53	-1.27
		BIONO	-0.03	0.19	-0.74	-1.26	-1.03	-1.06	2.25	2.72	1.28	0.08	-1.36	-0.63
		Red/Inc	-95.2	-54.71	-51.67	-47.51	-57.57	-65.08	73.2	79.12	13.22	-94.44	-46.41	-50.69
Wet Savannas	La	BASE	0.25	-0.84	-1.07	-0.76	-0.31	-0.36	-0.22	-0.35	-0.35	-0.27	0.21	0.51
		BIONO	0.95	-0.13	-0.46	-0.09	0.35	0.27	0.26	0.12	0.28	0.64	1.05	1.26
		Red/Inc	286.37	-84.14	-57.09	-87.57	11.55	-24.72	20.15	-64.49	-18.37	137.2	406.76	146.79
	Dj	BASE	1.59	-0.16	-0.54	-0.64	-0.4	-0.45	-0.2	0.4	0.66	0.95	-0.09	0.84
		BIONO	2.86	1.18	0.58	0.48	0.77	1	1.62	2.06	2.4	2.15	0.99	2.28
		Red/Inc	79.95	656.78	8.14	-25.51	91.97	121.09	716.21	410.01	264	126.18	1052.96	171.61
Forests	Bo	BASE	-0.80	-1.37	-1.17	-1.33	-1.64	-1.56	-0.98	-1.15	-1.12	-0.82	-0.55	0.16
		BIONO	0.20	-0.41	-0.23	-0.45	-0.77	-0.71	-0.13	-0.35	-0.39	-0.08	0.41	1.19
		Red/Inc	-75.32	-69.82	-80.71	-66.58	-52.96	-54.28	-86.47	-69.38	-65.42	-90.82	-24.59	649.99
	Zo	BASE	0.88	-1.04	-0.82	-0.74	-0.54	-0.45	0.03	-0.30	-0.36	-0.37	0.05	1.14
		BIONO	1.65	-0.19	0.13	0.21	0.35	0.26	0.60	0.18	0.30	0.40	1.00	1.99
		Red/Inc	87.84	-81.28	-83.92	-71.35	-35.02	-41.79	2046.86	-41.26	-17.48	7.11	1769.01	74.47

<sup>a</sup> Bias with BASE simulation

<sup>b</sup> Bias with BIONO simulation

<sup>c</sup> Reduction/Increase Bias by BioNO emissions



For tropical/transition forest ecosystems, both the BASE simulation and CAMS reanalysis show a significant  $\text{NO}_2$  underestimation compared to INDAAF measurements. The discrepancies observed in the BASE and CAMS simulations could be influenced by several factors, including the representation of  $\text{NO}_x$  sources such as anthropogenic emissions near the surface and regional chemical processes. Furthermore, INDAAF stations are often located in areas with strong simulated  $\text{NO}_2$  gradients (BIONO run), particularly in DJF, where even slight spatial discrepancies could lead to significant differences between simulated and observed levels (challenge of regional representativity of the INDAAF stations). The introduction of BioNO emissions in the simulation helps to reduce these discrepancies by enhancing  $\text{NO}_x$  concentrations, which in turn brings the simulated ozone levels closer to those observed (Figures 10 and 11).

### 450 6.1.2 $\text{HNO}_3$ concentration

On Figure 12, simulations exhibit in general a consistent representation of  $\text{HNO}_3$  spatial distributions between the different models. While RegCM concentrations are rather close to CAMS in magnitude, both are significantly smaller than Geos-Chem, in relation to the  $\text{O}_3$  fields as discussed later. Over the Sahel, the lower JJA simulated  $\text{HNO}_3$  concentrations (BASE run) are likely associated with the previously discussed underestimation of modelled  $\text{NO}_2$  in the regions ( $5^\circ$ - $20^\circ\text{N}$ ), since  $\text{HNO}_3$  is a product of  $\text{NO}_2$  oxidation. In general for both seasons, BioNO contribute to increased spatial concentrations of  $\text{HNO}_3$ , bringing RegCM simulations closer to reanalysis and Geos-Chem as shown by Figure 12.

According to Figure 9, the lower troposphere  $\text{HNO}_3$  increase can reach 0.3 ppb with maximum increases correlated with strong BioNO emissions (Figures 5a, 5d), as for  $\text{NO}_2$ . The effect of BioNO on  $\text{HNO}_3$  is somehow less sensitive compared to  $\text{NO}_2$ . This sensitivity difference is likely due to chemical controls occurring through OH and  $\text{O}_3$  formation (Steinkamp et al., 2009).  $\text{HNO}_3$  formation pathways from  $\text{NO}_2$  involve the presence of oxidants such as OH and  $\text{O}_3$ , which are controlled by regional photo-oxidant chemistry and emissions. As a result, the impact of BioNO on simulated  $\text{HNO}_3$  is not as straightforward as for  $\text{NO}_2$ .

As for  $\text{NO}_2$ , both RegCM5 and CAMS show an overall large underestimation of  $\text{HNO}_3$  concentrations compared to available measurements over nearly all INDAAF stations (Figure 13). The corresponding biases are large in the wet season and smaller in the dry season when the contribution of biomass burning is more important relative to BioNO (Figure 13/Table 6). The maximum bias in late June for wet season over dry savannas is likely to be partially due to the same reasons as discussed previously for the monthly-averaged  $\text{NO}_2$  concentrations. Lin et al. (2013) argue that enhanced soil emissions and higher  $\text{NO}_x$  oxidation rate under warmer conditions can generate high atmospheric  $\text{HNO}_3$ . Despite the large remaining underestimation, due to the less sensitive improvement across all ecosystems, the addition of BioNO in RegCM5 helps reduce the biases and brings the model closer to the observations (Figure 13). Figure 13 indicates an overall increase at all the study sites and a reduction in negative bias: a maximum of -1.67 vs -1.73 ppb in June (3.51% reduction in negative bias) in dry savannas, -0.77 vs -0.8 ppb in April (4.56% reduction in negative bias) in wet savannas, and around 2.27% reduction in negative bias over forests.

In addition to improving the amplitude of surface concentrations at the six remote sites and across the region, the introduction of ANN on-line emissions also improves the spatial correlation between the simulated (RegCM) and observed (INDAAF)



**Table 6.** BASE and BIONO Biases (ppb) for HNO<sub>3</sub>. The Reduced/Increased (Red/Inc) biases given by BIONO run is in %. Ba: Banizoumbou, Ka: Katibougou, La: Lamto, Dj: Djougou, Bo: Bomassa, Zoétélé: Zo

		Month												
		Jan	Feb	Mar	Apr	May	Jun	Jul	Aug	Sep	Oct	Nov	Dec	
Dry Savannas	Ba	BASE <sup>a</sup>		-0.02	-0.05	-0.25	-0.47	-1.36	-0.95	-0.91	-0.51	-0.46	-0.03	-0.05
		BIONO <sup>b</sup>		0.01	-0.04	-0.23	-0.45	-1.32	-0.87	-0.79	-0.36	-0.38	-0.01	-0.04
		Red/Inc <sup>c</sup>		-67.9	-12.35	-6.06	-4.02	-2.75	-8.47	-13.07	-29.26	-18.24	-68.23	-22.09
	Ka	BASE		-0.68		-0.45	-1.18	-1.73	-0.41	-1.01	-0.54	-0.32	-0.14	0.02
		BIONO		-0.64		-0.40	-1.13	-1.67	-0.30	-0.90	-0.44	-0.23	-0.08	0.05
		Red/Inc		-5.75		-10.28	-4.31	-3.51	-25.82	-11.12	-19.24	-29.46	-43.56	148.94
Wet Savannas	La	BASE	-0.07	-0.53	-0.66	-0.52	-0.36	-0.45	-0.16	-0.12	-0.13	-0.19	-0.21	-0.03
		BIONO	0.03	-0.47	-0.63	-0.51	-0.34	-0.42	-0.12	-0.06	-0.09	-0.17	-0.17	0.05
		Red/Inc	-62.64	-10.56	-4.79	-3.34	-4.56	-5.77	-25.28	-47.81	-31.76	-12.32	-20.27	53.7
	Dj	BASE	0.26	-0.27	-0.39	-0.80	-0.68	-0.41	-0.30	-0.54	-0.35	-0.41	-0.27	-0.08
		BIONO	0.36	-0.20	-0.35	-0.77	-0.65	-0.36	-0.23	-0.48	-0.31	-0.34	-0.17	0.01
		Red/Inc	38.57	-26.36	-10.94	-4.56	-5.10	-12.64	-23.90	-10.38	-11.09	-16.50	-37.03	-84.93
Forests	Bo	BASE	-0.27	-0.42	-0.54	-0.45	-0.37	-0.24	-0.34	-0.35	-0.41	-0.17	-0.43	-0.16
		BIONO	-0.23	-0.40	-0.52	-0.44	-0.36	-0.24	-0.33	-0.34	-0.41	-0.17	-0.42	-0.13
		Red/Inc	-13.69	-4.99	-2.27	-1.25	-1.57	-2.68	-2.60	-1.98	-0.43	-0.52	-2.67	-19.02
	Zo	BASE	0.05	-0.38	-0.26	-0.26	-0.25	-0.44	-0.10	-0.26	-0.18	-0.09	-0.27	-0.13
		BIONO	0.09	-0.36	-0.24	-0.26	-0.24	-0.43	-0.09	-0.25	-0.17	-0.09	-0.26	-0.09
		Red/Inc	84.56	-4.46	-4.67	-2.39	-1.46	-1.22	-7.70	-2.93	-2.48	-1.86	-4.61	-31

<sup>a</sup> Bias with BASE simulation

<sup>b</sup> Bias with BIONO simulation

<sup>c</sup> Reduction/Increase Bias by BioNO emissions

concentrations. The BioNO induced enhancement is also associated with a more realistic seasonal evolution of NO<sub>2</sub> and HNO<sub>3</sub> surface levels when compared to INDAAF observations (Figures 11 and 14).

## 6.2 Regional and local Ozone

Together with transport, emission and deposition processes, ozone photo-chemistry regulates the content of nitrogen compounds in the atmosphere. Tropospheric Ozone simulation is in general very challenging due to numerous sources of variability and uncertainties (Young et al., 2018). Such simulations involve complex and interrelated factors, including precursor emissions, meteorological variability, ozone photochemical production and loss, surface deposition, long-range transport influence



and stratosphere-troposphere exchange (Lelieveld and Dentener, 2000). In this section we discuss the ability of the model to represent regional ozone and the subsequent impact of BioNO emissions on regional ozone production. Figure 15 displays the regional surface ozone simulated by RegCM5-CHEM for BASE and BioNO runs, compared to the CAMS chemical reanalysis and the Geos-Chem model. The strong seasonality of surface ozone concentrations (winter vs summer) is first highlighted.

In the DJF season, strong ozone production occurs between 5°N and 15°N as a result of biomass burning activities. RegCM5-CHEM shows a consistent spatial pattern with CAMS and Geos-Chem in terms of simulated surface concentrations, but with lower values in the source zones (Geos-Chem showing the larger concentrations). In areas where local chemical production is low such as over the Sahara, long range and vertical ozone transport essentially determines the background ozone level (e.g., Sauvage et al., 2005). We can outline here the added values of improved chemical boundary conditions which set up a realistic and climatically relevant seasonal ozone background compared to CAMS reanalysis, while also accounting for long range transport events at shorter time scale.

During summer months (JJA), we also observe consistency between the continental-scale surface ozone gradients simulated by RegCM5 and those from CAMS and Geos-Chem. In northern Africa, there is a only a slight overestimation of ozone, which can be attributed to enhanced vertical transport and mixing during the African monsoon (the south-to-north transport more effective, Sauvage et al., 2007), potentially combined with an overrepresentation of stratosphere-troposphere exchange and local photochemical production under strong solar radiation (Li et al., 2019). However, in the southern biomass burning regions ozone “hot-spots” (Sauvage et al., 2007), RegCM5 tends to simulate lower surface ozone concentrations compared to CAMS and more noticeably, to Geos-Chem.

Focusing here on surface concentration only offers a limited view of actual model to model differences, and a deeper tropospheric ozone budget assessment would be required for a more systematic quantitative analysis, which is beyond the scope of this paper. Studies have shown that discrepancies in model ozone simulations are in general large in tropical regions. For example, a comprehensive intercomparison between Geos-Chem and CAM-chem (e.g., Lin et al., 2024) highlighted significant differences in ozone budgets and vertical profiles due to variations in photolysis schemes, aerosol interactions, and convective transport processes. These differences can lead to variations in how ozone is transported vertically, impacting surface concentrations (e.g., Li et al., 2019). Moreover, recent intercomparison studies focusing on tropospheric ozone in various tropical regions, including Africa, confirm that such discrepancies are common and often linked to model-specific handling of emissions, injection heights and vertical dynamics (Huijnen et al., 2020; Lin et al., 2024). For instance, Tsvilidou et al. (2023) argue that it is essential to consider the combination of injection height of ozone precursors and the strong vertical mixing in the tropics which largely determine the surface ozone values. These factors, along with the non-linear interactions between NO<sub>x</sub> and VOCs, including the uncertain biogenic emissions, must be carefully analysed when assessing model outputs.

Figures 16c and 16f illustrate the influence of BioNO emissions on the RegCM5 simulated surface O<sub>3</sub> field. The consecutive production or depletion of O<sub>3</sub> is not solely dependent on NO<sub>x</sub> concentrations but also on the NO<sub>x</sub>/VOCs ratio, which determines the ozone chemical regime variable in different subregions of the domain. At the regional to continental scale and for both seasons, the introduction of BioNO leads to both an increase and a decrease in surface ozone production, with a predominantly increasing effect in the lower troposphere (Figures 9c,f and 16c,f). In regions coinciding with intense BioNO emissions



and for both seasons, there is however a notable negative impact on surface  $O_3$ . This decrease in ozone levels, which can reach up to 2 ppb, is likely due to ozone titration processes, more characteristic of VOC-limited conditions. In areas with higher proportion of  $NO_x$  emissions (here BioNO source areas),  $O_3$  formation can be VOC-limited or may shift between chemical regimes (Kleinman, 1994; Sillman and He, 2002) e.g depending on the time of the day.

As one moves away from these intense sources towards the regional scale, the ozone average response shifts to positive, reflecting the classical change in chemical regime downwind of the sources. An illustration of this process can be seen in JJA in the vertical wind (wa) monsoon region where intense Sahelian BioNO sources decrease locally surface ozone but contribute to a relative downwind surface ozone increase in northern Sahel/southern Sahara (dipole pattern on Figure 16f). For this situation,  $NO_x/VOC$  ratio decreases and chemical regime becomes more  $NO_x$ -limited (Delon et al., 2008; Stewart et al., 2008). In DJF, the surface ozone increase can reach approximately 4 ppb in the southern part of the domain, while in JJA, we observe increases of up to 3 ppb over the Sahel region and in eastern Africa. Over West Africa, this influence extends into the lower troposphere, where an average increase in ozone concentration of up to 4 ppb is noted (Figure 9c,f). This pattern aligns with findings by De- lon et al. (2008), who observed that a moderate increase in  $NO_x$  concentrations leads to a sensitive increase in simulated ozone across all altitudes (0-15 km), characteristic of a  $NO_x$ -limited regime. Several studies have shown that throughout much of the troposphere in tropical regions, including Africa,  $O_3$  formation is predominantly  $NO_x$ -limited, meaning it largely depends on the availability of  $NO_x$  (e.g., Li et al., 2021; Tadic et al., 2021).

Regarding comparison with the INDAAF ozone ground measurements, Figure 17 indicates that, unlike the improvements observed for other species, the inclusion of BioNO emissions results in minimal to no enhancement in simulated ozone concentrations at the local level. However, a general reduction in bias, leading to better alignment between simulated and observed values, is observed for nearly all the sites during the period from June to August. In dry savannas the maximum negative bias is for instance reduced by 83.38 % in June over Banizoumbou (Table 7) while the ozone increase can also contribute to worsen the positive bias (+2.4 % in march). We observe an overall slight decrease in  $O_3$  amplitude induced by BioNO over wet savannas and equatorial forests from June to August, which tends to only very moderately improve simulations. Over tropical forest surface ozone concentrations are influenced by regional transport from burning areas, and local vertical exchanges between surface and lower troposphere. Model-measurement  $O_3$  comparisons are not straightforward due to the presence of an important tree canopy on measurement sites (<https://doi.org/10.25326/607>; <https://doi.org/10.25326/603>) which can potentially affects both local dynamics and chemistry (e.g., Bryan and Steiner, 2013). Big leaf dry deposition schemes for ozone over tropical forests can only crudely represent deposition processes, while extra chemical sinks within the canopy layer are simply not properly parametrized (Ganzeveld and Lelieveld, 2004; Sun et al., 2022). These deposition and chemical processes in the canopy should potentially be accounted for to better explain the discrepancy between the simulations and the in situ observations, and notably the fact that ozone observations are systematically much lower than model results in general (Figures 17 and 18).



**Table 7.** BASE and BIONO Biases (ppb) for O<sub>3</sub>. The Reduced/Increased (Red/Inc) biases given by BIONO run is in %. Ba: Banizoumbou, Ka: Katibougou, La: Lamto, Dj: Djougou, Bo: Bomassa, Zoétélé: Zo

		Month												
		Jan	Feb	Mar	Apr	May	Jun	Jul	Aug	Sep	Oct	Nov	Dec	
Dry Savannas	Ba	BASE <sup>a</sup>	29.19	29.69	34.20	20.44	7.01	-2.46	-1.29	-1.06	6.64	12.16	28.46	26.72
		BIONO <sup>b</sup>	29.15	29.94	35.02	22.24	9.04	-0.41	-1.00	-1.98	9.28	14.56	29.08	26.87
		Red/Inc <sup>c</sup>	-0.16	0.83	2.40	8.78	28.84	-83.38	-22.87	86.79	39.70	19.67	2.16	0.54
	Ka	BASE	30.44	26.04	29.86	19.01	-2.64	-9.84	12.94	1.97	7.22	13.00	20.23	29.63
		BIONO	29.93	25.80	29.53	19.42	-1.23	-8.80	13.35	2.25	10.11	15.59	20.23	29.34
		Red/Inc	-1.68	-0.93	-1.09	2.17	-53.40	-10.53	3.19	14.00	40.03	19.91	-0.03	-0.97
Wet savannas	La	BASE	20.45	11.04	7.34	3.78	7.05	15.40	26.23	28.72	24.33	11.89	10.63	14.54
		BIONO	20.77	11.56	8.83	5.70	7.74	15.43	26.18	28.83	23.80	12.02	11.66	15.22
		Red/Inc	1.56	4.72	20.40	50.89	9.80	0.19	-0.21	0.38	-2.17	1.15	9.68	4.65
	Dj	BASE	24.57	15.22	5.51	-2.63	-1.98	2.01	11.17	11.83	6.95	5.58	9.82	17.57
		BIONO	24.17	15.12	6.36	-0.58	-0.52	2.46	10.28	10.73	6.93	7.39	10.61	17.25
		Red/Inc	-1.64	-0.63	15.52	-78.09	-73.72	22.54	-7.94	-9.33	-0.25	32.48	8.10	-1.87
Forest	Bo	BASE	17.38	11.39	6.39	4.63	7.74	12.04	15.46	14.91	5.08	1.96	5.80	17.08
		BIONO	17.86	12.20	8.32	6.27	8.16	11.66	15.08	14.57	5.02	3.11	7.57	17.83
		Red/Inc	2.77	7.12	30.28	35.51	5.45	-3.15	-2.44	-2.30	-1.16	58.58	30.44	4.39
	Zo	BASE	18.57	6.10	5.01	4.23	2.64	9.56	19.67	23.05	13.45	4.61	4.24	14.92
		BIONO	19.14	6.69	6.31	6.08	3.57	9.65	19.40	23.04	13.02	5.33	6.11	15.39
		Red/Inc	3.09	9.70	26.07	43.94	35.60	0.91	-1.34	-0.07	-3.20	15.57	44.12	3.21

<sup>a</sup> Bias with BASE simulation

<sup>b</sup> Bias with BIONO simulation

<sup>c</sup> Reduction/Increase Bias by BioNO emissions

## 7 Conclusion

550 RegCM5 is the latest released version of the ICTP regional climate model designed to conduct high-resolution regional climate simulations. In the broader context of on-going programs targeting the regional nitrogen cycle over Africa, we more specifically use and assess the related atmospheric chemistry module (RegCM5-Chem), which has been substantially updated relative to previous versions. Doing so, we also conduct a specific study targeting the impact of BioNO emissions on regional chemistry over Africa. The sensitivity study consists of two experiments of 3-years coupled climate chemistry runs considering or not

555 BioNO emissions, simulated through an original parameterization based on ANN. These runs, and the impact of BioNO are





evaluated in the light of various data including satellite observations for climate, ground-based observations, reanalysis and alternative state of the art model outputs for key atmospheric compounds.

Obtained results show evidence that RegCM5-CHEM can capture the main features of the regional climate over the region, for instance in terms of seasonal and daily mean of temperature, precipitation and wind circulation relevant for regional atmospheric chemistry and emission processes.

Simulated  $\text{NO}_2$ ,  $\text{HNO}_3$  and  $\text{O}_3$  fields show consistency with reanalysis and Geos-Chem simulations in terms of spatio-temporal distribution and gradients. Local comparison with surface concentrations measured over the six INDAAF sites indicates that the coupled chemistry-climate model can reproduce the seasonal cycle of all species over all sites. However, these comparisons strikingly outline an overall overestimation of simulated  $\text{O}_3$  and, to a lesser extent, an underestimation of  $\text{NO}_2$  and  $\text{HNO}_3$  especially in the wet season over dry savannas stations. These large biases are present not only in RegCM simulations but also in reanalyses, and Geos-Chem outputs. In BASE simulation, the  $\text{O}_3$  biases range from -2.64 to 34.2 ppb (dry savannas), -2.63 to 28.72 ppb (wet savannas) and 1.96 to 23.05 ppb (forests) while for  $\text{NO}_2$ , we obtained biases from -4.97 to -0.41 ppb (dry savannas), -0.84 to 1.59 ppb (wet savannas), -1.64 to 1.14 ppb (forests), and -1.73 to 0.02 ppb (dry savannas), -0.8 to 0.26 (wet savannas) and -0.54 to 0.05 ppb (forests) for  $\text{HNO}_3$ . These differences are attributed to potential deficiencies in chemical emissions and mechanisms, deposition, boundary layer dynamics and transport from the upper layer which are particularly challenging to be reproduced in tropical regions. It is well known that regional models often struggle to accurately capture local-scale emissions and processes due to the coarse resolution (Valari and Menut, 2008; Wang et al., 2023) of their grids (in this case, 30 km x 30 km), which can lead to discrepancies when comparing with point measurements. Nevertheless, despite a substantial room for potential improvements, our conclusion is that RegCM5-Chem performance turns out to be consistent with state of the art chemical reanalysis and chemistry transport model regarding regional photo-oxidant chemistry.

When integrating BioNO emissions, we estimate seasonal averaged BioNO flux to be ranging from 0.02 to 7  $\text{mg m}^{-2} \text{day}^{-1}$  and a total amount of nitrogen emitted from BioNO ranging from 0.01 to 4.4  $\text{TgN. month}^{-1}$  on the whole domain. The regional distribution of BioNO is essentially determined by the environmental predictors considered in the ANN based parameterization, with an important role of soil moisture variability. When taken into account, BioNO emissions lead to increased concentration levels of surface  $\text{NO}_2$  (ranging from 0.05 to 4 ppb) and  $\text{HNO}_3$  (from 0.05 to 0.3). A decrease in surface ozone (until 2 ppb likely in the Sahel) is also obtained as a likely result of predominant NO induced titration effect in the surface layer, while the  $\text{O}_3$  concentrations relatively increase in altitude and downwind from BioNO sources and towards the regional scale (up to 4 ppb).

In terms of model performance compared to INDAAF stations, the inclusion of BioNO emissions improves the representation of  $\text{O}_3$ ,  $\text{NO}_2$ , and  $\text{HNO}_3$  seasonal cycles and concentration magnitudes, particularly by reducing biases in some cases. However, in certain conditions, it can also lead to an increase in biases, highlighting the complex interactions at play across different regions and ecosystems.

Overall, our study points out an added value of including interactive BioNO emission representations, especially over the dry savannas of northern Sahel, where atmospheric nitrogen cycle and deposition inputs are particularly important for these ecosystems where N content is low and sensitive to small variations. One limitation of the ANN approach is that it does not



account for limitations in the nitrogen pool ready to be emitted, which could be at play especially in dryer and unfertilized ecosystems. A deeper look at such limitations, using for example constraints from explicit soil nitrogen modules, is foreseen. Perspective to this work also include improving the representation of atmospheric chemistry processes important for the regional nitrogen budgets, such as LiNO<sub>x</sub> emissions and relevant heterogeneous chemistry processes (e.g. dust - HNO<sub>3</sub>), which will have a significant impact on deposition processes, while keeping numerical efficiency required by climate scale simulation. Extended multi-decadal simulations aiming at investigating the impacts of regional climate variability and direct anthropogenic perturbations on the regional nitrogen cycle over Africa, which may bring a more thorough insight in future trends of these processes in Africa.

*Code and data availability.* The RegCM5 model code can be accessed at the web site: <https://zenodo.org/record/7548172#.Y8gVV7TM-KUK.INDAAF> measurement network data is available at <https://indaaf.obs-mip.fr>. OMI TROPOMI-inferred ground-level NO<sub>2</sub> concentrations from 2010 to 2013 used in this study are available at <https://doi.org/10.5281/zenodo.5424752>. The GEOS-Chem model version 12.9.3 used in this work is available at <https://doi.org/10.5281/zenodo.3974569>. Data from these simulations can be freely shared upon request via email to [fabien.solmon@aero.obs-mip.fr](mailto:fabien.solmon@aero.obs-mip.fr)

*Author contributions.* EMY designed and conducted the research under the supervision of FS and MA. with CD, CGL, BS and GG acting as advisors. Methodology and original draft preparation were handled by EMY and FS. Writing, review, and editing were completed by MA, CD, CGL, BS and VY.

*Competing interests.* The authors declare that they have no financial or personal conflicts that could have affected the integrity of the work presented in this paper.

*Acknowledgements.* This work was funded by the European Horizon 2020 project 'Marie Skłodowska-Curie Actions-Research and Innovation Staff Exchange Integrated Nitrogen Studies in Africa' (H2020 MSCA-RISE INSA, GA 871944; <https://doi.org/10.3030/871944>). The authors would like to acknowledge the INDAAF project (International Network to study Deposition and Atmospheric chemistry in Africa) supported by the INSU (Institut National des Sciences de l'Univers) /CNRS (Centre National de la Recherche Scientifique), IRD (Institut de Recherche pour le Développement) and the research infrastructure ACTRIS-FR registered on the Roadmap of the French Ministry of Research. We also express our gratitude to all INDAAF local technicians for their maintenance and sampling work. We also acknowledge the use of the CALMIP (CALcul du Midi-Pyrénées) computing resources, supported by CNRS, Toulouse INP, INSA Toulouse, ISAE Supaero, and UT3 Paul Sabatier (UAR 3667; <https://www.calmip.univ-toulouse.fr/node/1>) for performing the numerical calculations presented in this paper.



## References

- Adon, M., Galy-Lacaux, C., Yoboué, V., Delon, C., Lacaux, J., Castera, P., Gardrat, E., Pienaar, J., Al Ourabi, H., Laouali, D., et al.: Long  
620 term measurements of sulfur dioxide, nitrogen dioxide, ammonia, nitric acid and ozone in Africa using passive samplers, *Atmospheric  
Chemistry and Physics*, 10, 7467–7487, <https://doi.org/10.5194/acp-10-7467-2010>, 2010.
- Adon, M., Galy-Lacaux, C., Delon, C., Yoboue, V., Solmon, F., and Kaptue Tchuenta, A.: Dry deposition of nitrogen compounds (NO<sub>2</sub>,  
HNO<sub>3</sub>, NH<sub>3</sub>), sulfur dioxide and ozone in west and central African ecosystems using the inferential method, *Atmospheric Chemistry  
and Physics*, 13, 11 351–11 374, <https://doi.org/10.5194/acp-13-11351-2013>, 2013.
- 625 Aghedo, A. M., Schultz, M. G., and Rast, S.: The influence of African air pollution on regional and global tropospheric ozone, *Atmospheric  
Chemistry and Physics*, 7, 1193–1212, <https://doi.org/10.5194/acp-7-1193-2007>, 2007.
- Austin, A. T., Yahdjian, L., Stark, J. M., Belnap, J., Porporato, A., Norton, U., Ravetta, D. A., and Schaeffer, S. M.: Water pulses and  
biogeochemical cycles in arid and semiarid ecosystems, *Oecologia*, 141, 221–235, <https://doi.org/10.1007/s00442-004-1519-1>, 2004.
- Bahino, J., Yoboué, V., Galy-Lacaux, C., Adon, M., Akpo, A., Keita, S., Liousse, C., Gardrat, E., Chiron, C., Ossohou, M., et al.: A pilot  
630 study of gaseous pollutants' measurement (NO<sub>2</sub>, SO<sub>2</sub>, NH<sub>3</sub>, HNO<sub>3</sub> and O<sub>3</sub>) in Abidjan, Côte d'Ivoire: contribution to an overview  
of gaseous pollution in African cities, *Atmospheric Chemistry and Physics*, 18, 5173–5198, <https://doi.org/10.5194/acp-18-5173-2018>,  
2018.
- Ban, N., Caillaud, C., Coppola, E., Pichelli, E., Sobolowski, S., Adinolfi, M., Ahrens, B., Alias, A., Anders, I., Bastin, S., et al.: The first  
multi-model ensemble of regional climate simulations at kilometer-scale resolution, part I: evaluation of precipitation, *Climate Dynamics*,  
635 57, 275–302, <https://doi.org/10.1007/s00382-021-05708-w>, 2021.
- Bretherton, C. S., McCaa, J. R., and Grenier, H.: A new parameterization for shallow cumulus convection and its application to  
marine subtropical cloud-topped boundary layers. Part I: Description and 1D results, *Monthly weather review*, 132, 864–882,  
[https://doi.org/10.1175/1520-0493\(2004\)132<0864:ANPFSC>2.0.CO;2](https://doi.org/10.1175/1520-0493(2004)132<0864:ANPFSC>2.0.CO;2), 2004.
- Bryan, A. M. and Steiner, A. L.: Canopy controls on the forest-atmosphere exchange of biogenic ozone and aerosol precursors, *Michigan  
640 Journal of Sustainability*, 1, <https://doi.org/10.3998/mjs.12333712.0001.005>, 2013.
- Bucchignani, E., Mercogliano, P., Panitz, H.-J., and Montesarchio, M.: Climate change projections for the Middle East–  
North Africa domain with COSMO-CLM at different spatial resolutions, *Advances in Climate Change Research*, 9, 66–80,  
<https://doi.org/10.1016/j.accre.2018.01.004>, 2018.
- Butterbach-Bahl, K., Kock, M., Willibald, G., Hewett, B., Buhagiar, S., Papen, H., and Kiese, R.: Temporal variations of fluxes of NO, NO<sub>2</sub>,  
645 N<sub>2</sub>O, CO<sub>2</sub>, and CH<sub>4</sub> in a tropical rain forest ecosystem, *Global Biogeochemical Cycles*, 18, <https://doi.org/10.1029/2004GB002243>,  
2004.
- Carmichael, G. R., Ferm, M., Thongboonchoo, N., Woo, J.-H., Chan, L., Murano, K., Viet, P. H., Mossberg, C., Bala, R., Boonjawat, J.,  
et al.: Measurements of sulfur dioxide, ozone and ammonia concentrations in Asia, Africa, and South America using passive samplers,  
*Atmospheric Environment*, 37, 1293–1308, [https://doi.org/10.1016/S1352-2310\(02\)01009-9](https://doi.org/10.1016/S1352-2310(02)01009-9), 2003.
- 650 Charusombat, U., Niyogi, D., Kumar, A., Wang, X., Chen, F., Guenther, A., Turnipseed, A., and Alapaty, K.: Evaluating a new deposition  
velocity module in the Noah land-surface model, *Boundary-layer meteorology*, 137, 271–290, <https://doi.org/10.1007/s10546-010-9531-y>,  
2010.
- Chauvin, F., Roehrig, R., and Lafore, J.-P.: Intraseasonal variability of the Saharan heat low and its link with midlatitudes, *Journal of Climate*,  
23, 2544–2561, <https://doi.org/10.1175/2010JCLI3093.1>, 2010.



- 655 Ciarlo, J., Aquilina, N., Strada, S., Shalaby, A., and Solmon, F.: A modified gas-phase scheme for advanced regional climate modelling with RegCM4, *Climate Dynamics*, 57, 489–502, <https://doi.org/10.1007/s00382-021-05722-y>, 2021.
- Cooper, M. J., Martin, R. V., McLinden, C. A., and Brook, J. R.: Inferring ground-level nitrogen dioxide concentrations at fine spatial resolution applied to the TROPOMI satellite instrument, *Environmental Research Letters*, 15, 104 013, <https://doi.org/10.1088/1748-9326/aba3a5>, 2020.
- 660 Cooper, M. J., Martin, R. V., Hammer, M. S., Levelt, P. F., Veefkind, P., Lamsal, L. N., Krotkov, N. A., Brook, J. R., and McLinden, C. A.: Global fine-scale changes in ambient NO<sub>2</sub> during COVID-19 lockdowns, *Nature*, 601, 380–387, <https://doi.org/10.1038/s41586-021-04229-0>, 2022.
- Coppola, E., Sobolowski, S., Pichelli, E., Raffaele, F., Ahrens, B., Anders, I., Ban, N., Bastin, S., Belda, M., Belusic, D., et al.: A first-of-its-kind multi-model convection permitting ensemble for investigating convective phenomena over Europe and the Mediterranean, *Climate Dynamics*, 55, 3–34, <https://doi.org/10.1007/s00382-018-4521-8>, 2020.
- 665 Davidson, E. A. and Kinglerlee, W.: A global inventory of nitric oxide emissions from soils, *Nutrient cycling in agroecosystems*, 48, 37–50, <https://doi.org/10.1023/A:1009738715891>, 1997.
- Davidson, E. A., Keller, M., Erickson, H. E., Verchot, L. V., and Veldkamp, E.: Testing a conceptual model of soil emissions of nitrous and nitric oxides: using two functions based on soil nitrogen availability and soil water content, the hole-in-the-pipe model characterizes a large fraction of the observed variation of nitric oxide and nitrous oxide emissions from soils, *Bioscience*, 50, 667–680, [https://doi.org/10.1641/0006-3568\(2000\)050\[0667:TACMOS\]2.0.CO;2](https://doi.org/10.1641/0006-3568(2000)050[0667:TACMOS]2.0.CO;2), 2000.
- Davolio, S., Malguzzi, P., Drofa, O., Mastrangelo, D., and Buzzi, A.: The Piedmont flood of November 1994: A testbed of forecasting capabilities of the CNR-ISAC meteorological model suite, *Bulletin of Atmospheric Science and Technology*, 1, 263–282, 2020.
- 675 Delmas, R., Peuch, V.-H., Mégie, G., and Brasseur, G. P.: Emissions anthropiques et naturelles et dépôts, in: *Physique et chimie de l’atmosphère*, edited by Belin, chap. 5, ISBN 2-7011-3700-4, in French, 1995.
- Delon, C., Serça, D., Boissard, C., Dupont, R., Dutot, A., Laville, P., De Rosnay, P., and Delmas, R.: Soil NO emissions modelling using artificial neural network, *Tellus B: Chemical and Physical Meteorology*, 59, 502–513, <https://doi.org/10.1111/j.1600-0889.2007.00254.x>, 2007.
- 680 Delon, C., Reeves, C., Stewart, D., Serça, D., Dupont, R., Mari, C., Chaboureau, J.-P., and Tulet, P.: Biogenic nitrogen oxide emissions from soils–impact on NO<sub>x</sub> and ozone over West Africa during AMMA (African Monsoon Multidisciplinary Experiment): modelling study, *Atmospheric Chemistry and Physics*, 8, 2351–2363, <https://doi.org/10.5194/acp-8-2351-2008>, 2008.
- Delon, C., Galy-Lacaux, C., Boone, A., Liousse, C., Serça, D., Adon, M., Diop, B., Akpo, A., Lavenu, F., Mougin, E., et al.: Atmospheric nitrogen budget in Sahelian dry savannas, *Atmospheric Chemistry and Physics*, 10, 2691–2708, 2010.
- 685 Delon, C., Galy-Lacaux, C., Adon, M., Liousse, C., Serça, D., Diop, B., and Akpo, A.: Nitrogen compounds emission and deposition in West African ecosystems: comparison between wet and dry savanna, *Biogeosciences*, 9, 385–402, <https://doi.org/10.5194/bg-9-385-2012>, 2012.
- Delon, C., Mougin, E., Serça, D., Grippa, M., Hiernaux, P., Diawara, M., Galy-Lacaux, C., and Kergoat, L.: Modelling the effect of soil moisture and organic matter degradation on biogenic NO emissions from soils in Sahel rangeland (Mali), *Biogeosciences*, 12, 3253–3272, <https://doi.org/10.5194/bg-12-3253-2015>, 2015.
- 690 Delon, C., Galy-Lacaux, C., Serça, D., Loubet, B., Camara, N., Gardrat, E., Saneh, I., Fensholt, R., Tagesson, T., Le Dantec, V., et al.: Soil and vegetation-atmosphere exchange of NO, NH<sub>3</sub>, and N<sub>2</sub>O from field measurements in a semi arid grazed ecosystem in Senegal, *Atmospheric Environment*, 156, 36–51, <https://doi.org/10.1016/j.atmosenv.2017.02.024>, 2017.



- Dickinson, R. E.: Biosphere/atmosphere transfer scheme (BATS) for the NCAR community climate model, Technical report, National Center for Research., <https://cir.nii.ac.jp/crid/1574231873842566272>, 1986.
- 695 Emmons, L. K., Walters, S., Hess, P. G., Lamarque, J.-F., Pfister, G. G., Fillmore, D., Granier, C., Guenther, A., Kinnison, D., Laepple, T., et al.: Description and evaluation of the Model for Ozone and Related chemical Tracers, version 4 (MOZART-4), *Geoscientific Model Development*, 3, 43–67, <https://doi.org/10.5194/gmd-3-43-2010>, 2010.
- Evan, A. T., Flamant, C., Lavaysse, C., Kocha, C., and Saci, A.: Water vapor–forced greenhouse warming over the Sahara Desert and the recent recovery from the Sahelian drought, *Journal of Climate*, 28, 108–123, <https://doi.org/10.1175/JCLI-D-14-00039.1>, 2015.
- 700 Feig, G., Mamtimin, B., and Meixner, F.: Soil biogenic emissions of nitric oxide from a semi-arid savanna in South Africa, *Biogeosciences*, 5, 1723–1738, <https://doi.org/10.5194/bg-5-1723-2008>, 2008.
- Ferm, M. and Rodhe, H.: Measurements of air concentrations of SO<sub>2</sub>, NO<sub>2</sub> and NH<sub>3</sub> at rural and remote sites in Asia, *Journal of Atmospheric Chemistry*, 27, 17–29, <https://doi.org/10.1023/A:1005816621522>, 1997.
- Ferm, M., Lindskog, A., Svanberg, P., and Boström, C.: New measurement technique for air pollutants, *Kemisk Tidskrift*, 1, 30–32, 1994.
- 705 Fountoukis, C. and Nenes, A.: ISORROPIA II: a computationally efficient thermodynamic equilibrium model for K<sup>+</sup>–Ca<sup>2+</sup>–Mg<sup>2+</sup>–NH<sub>4</sub><sup>+</sup>–Na<sup>+</sup>–SO<sub>4</sub><sup>2-</sup>–NO<sub>3</sub><sup>-</sup>–Cl<sup>-</sup>–H<sub>2</sub>O aerosols, *Atmospheric Chemistry and Physics*, 7, 4639–4659, <https://doi.org/10.5194/acp-7-4639-2007>, 2007.
- Fudjoe, S. K., Li, L., Anwar, S., Shi, S., Xie, J., Wang, L., Xie, L., and Yongjie, Z.: Nitrogen fertilization promoted microbial growth and N<sub>2</sub>O emissions by increasing the abundance of nirS and nosZ denitrifiers in semiarid maize field, *Frontiers in Microbiology*, 14, 1265 562, <https://doi.org/10.3389/fmicb.2023.1265562>, 2023.
- 710 Galloway, J. N., Townsend, A. R., Erisman, J. W., Bekunda, M., Cai, Z., Freney, J. R., Martinelli, L. A., Seitzinger, S. P., and Sutton, M. A.: Transformation of the nitrogen cycle: recent trends, questions, and potential solutions, *Science*, 320, 889–892, <https://doi.org/10.1126/science.113667>, 2008.
- Galy-Lacaux, C. and Modi, A.: Precipitation chemistry in the Sahelian savanna of Niger, Africa, *Journal of atmospheric chemistry*, 30, 319–343, <https://doi.org/10.1023/A:1006027730377>, 1998.
- Galy-Lacaux, C., Laouali, D., Descroix, L., Gobron, N., and Liousse, C.: Long term precipitation chemistry and wet deposition in a remote dry savanna site in Africa (Niger), *Atmospheric Chemistry and Physics*, 9, 1579–1595, <https://doi.org/10.5194/acp-9-1579-2009>, 2009.
- Ganzeveld, L. and Lelieveld, J.: Impact of Amazonian deforestation on atmospheric chemistry, *Geophysical Research Letters*, 31, <https://doi.org/10.1029/2003GL019205>, 2004.
- 720 Ganzeveld, L., Lelieveld, J., Dentener, F., Krol, M., Bouwman, A., and Roelofs, G.-J.: Global soil-biogenic NO<sub>x</sub> emissions and the role of canopy processes, *Journal of Geophysical Research: Atmospheres*, 107, ACH–9, <https://doi.org/10.1029/2001JD000684>, 2002.
- Gasche, R. and Papen, H.: A 3-year continuous record of nitrogen trace gas fluxes from untreated and limed soil of a N-saturated spruce and beech forest ecosystem in Germany: 2. NO and NO<sub>2</sub> fluxes, *Journal of Geophysical Research: Atmospheres*, 104, 18 505–18 520, <https://doi.org/10.1029/1999JD900294>, 1999.
- 725 Giorgi, F., Coppola, E., Giuliani, G., Ciarlo, J. M., Pichelli, E., Nogherotto, R., Raffaele, F., Malguzzi, P., Davolio, S., Stocchi, P., et al.: The fifth generation regional climate modeling system, RegCM5: Description and illustrative examples at parameterized convection and convection-permitting resolutions, *Journal of Geophysical Research: Atmospheres*, 128, e2022JD038 199, <https://doi.org/10.1029/2022JD038199>, 2023.
- Granier, C., Pétron, G., Müller, J.-F., and Brasseur, G.: The impact of natural and anthropogenic hydrocarbons on the tropospheric budget of carbon monoxide, *Atmospheric Environment*, 34, 5255–5270, [https://doi.org/10.1016/S1352-2310\(00\)00299-5](https://doi.org/10.1016/S1352-2310(00)00299-5), 2000.
- 730



- Guenther, A., Karl, T., Harley, P., Wiedinmyer, C., Palmer, P. I., and Geron, C.: Estimates of global terrestrial isoprene emissions using MEGAN (Model of Emissions of Gases and Aerosols from Nature), *Atmospheric Chemistry and Physics*, 6, 3181–3210, <https://doi.org/10.5194/acp-6-3181-2006>, 2006.
- Harris, I., Osborn, T. J., Jones, P., and Lister, D.: Version 4 of the CRU TS monthly high-resolution gridded multivariate climate dataset, *Scientific data*, 7, 109, <https://doi.org/10.1038/s41597-020-0453-3>, 2020.
- Hersbach, H., Bell, B., Berrisford, P., Hirahara, S., Horányi, A., Muñoz-Sabater, J., Nicolas, J., Peubey, C., Radu, R., Schepers, D., et al.: The ERA5 global reanalysis, *Quarterly Journal of the Royal Meteorological Society*, 146, 1999–2049, <https://doi.org/10.1002/qj.3803>, 2020.
- Hickman, J. E., Dammers, E., Galy-Lacaux, C., and Van der Werf, G. R.: Satellite evidence of substantial rain-induced soil emissions of ammonia across the Sahel, *Atmospheric Chemistry and Physics*, 18, 16 713–16 727, <https://doi.org/10.5194/acp-18-16713-2018>, 2018.
- 740 Horowitz, L. W., Walters, S., Mauzerall, D. L., Emmons, L. K., Rasch, P. J., Granier, C., Tie, X., Lamarque, J.-F., Schultz, M. G., Tyndall, G. S., et al.: A global simulation of tropospheric ozone and related tracers: Description and evaluation of MOZART, version 2, *Journal of geophysical research: Atmospheres*, 108, <https://doi.org/10.1029/2002JD002853>, 2003.
- Hourdin, F., Musat, I., Guichard, F. s., Ruti, P. M., Favot, F., Filiberti, M.-A., Pham, M., Grandpeix, J.-Y., Polcher, J., Marquet, P., et al.: AMMA-model intercomparison project, *Bulletin of the American Meteorological Society*, 91, 95–104, <https://doi.org/10.1175/2009BAMS2791.1>, 2010.
- 745 Hudman, R., Moore, N., Mebust, A., Martin, R., Russell, A., Valin, L., and Cohen, R.: Steps towards a mechanistic model of global soil nitric oxide emissions: implementation and space based-constraints, *Atmospheric Chemistry and Physics*, 12, 7779–7795, <https://doi.org/10.5194/acp-12-7779-2012>, 2012.
- Huffman, G. J., Bolvin, D. T., Nelkin, E. J., Wolff, D. B., Adler, R. F., Gu, G., Hong, Y., Bowman, K. P., and Stocker, E. F.: The TRMM multisatellite precipitation analysis (TMPA): Quasi-global, multiyear, combined-sensor precipitation estimates at fine scales, *Journal of hydrometeorology*, 8, 38–55, <https://doi.org/10.1175/JHM560.1>, 2007.
- 750 Huijnen, V., Pozzer, A., Arteta, J., Brasseur, G., Bouarar, I., Chabrilat, S., Christophe, Y., Doumbia, T., Flemming, J., Guth, J., et al.: Quantifying uncertainties due to chemistry modelling–evaluation of tropospheric composition simulations in the CAMS model (cycle 43R1), *Geoscientific Model Development*, 12, 1725–1752, <https://doi.org/10.5194/gmd-12-1725-2019>, 2019.
- 755 Huijnen, V., Miyazaki, K., Flemming, J., Inness, A., Sekiya, T., and Schultz, M. G.: An intercomparison of tropospheric ozone reanalysis products from CAMS, CAMS interim, TCR-1, and TCR-2, *Geoscientific model development*, 13, 1513–1544, <https://doi.org/10.5194/gmd-13-1513-2020>, 2020.
- Igbb-Dis, S.: A program for creating global soil-property databases, IGBP Global Soils Data Task, France, 1998.
- Inness, A., Ades, M., Agustí-Panareda, A., Barré, J., Benedictow, A., Blechschmidt, A.-M., Dominguez, J. J., Engelen, R., Eskes, H., Flemming, J., et al.: The CAMS reanalysis of atmospheric composition, *Atmospheric Chemistry and Physics*, 19, 3515–3556, <https://doi.org/10.5194/acp-19-3515-2019>, 2019.
- 760 Jaeglé, L., Martin, R. V., Chance, K., Steinberger, L., Kurosui, T. P., Jacob, D. J., Modi, A., Yoboué, V., Sigha-Nkamdjou, L., and Galy-Lacaux, C.: Satellite mapping of rain-induced nitric oxide emissions from soils, *Journal of Geophysical Research: Atmospheres*, 109, <https://doi.org/10.1029/2004JD004787>, 2004.
- 765 Jaeglé, L., Steinberger, L., Martin, R. V., and Chance, K.: Global partitioning of NO<sub>x</sub> sources using satellite observations: Relative roles of fossil fuel combustion, biomass burning and soil emissions, *Faraday discussions*, 130, 407–423, <https://doi.org/10.1039/B502128F>, 2005.
- Johansson, C., Rodhe, H., and Sanhueza, E.: Emission of NO in a tropical savanna and a cloud forest during the dry season, *Journal of Geophysical Research: Atmospheres*, 93, 7180–7192, <https://doi.org/10.1029/JD093iD06p07180>, 1988.





- KhayatianYazdi, F., Kamali, G., Mirrokni, S. M., and Memarian, M. H.: Sensitivity evaluation of the different physical parameterizations schemes in regional climate model RegCM4. 5 for simulation of air temperature and precipitation over North and West of Iran, *Dynamics of Atmospheres and Oceans*, 93, 101–199, <https://doi.org/10.1016/j.dynatmoce.2020.101199>, 2021.
- 770 Kleinman, L. I.: Low and high NO<sub>x</sub> tropospheric photochemistry, *Journal of Geophysical Research: Atmospheres*, 99, 16 831–16 838, <https://doi.org/10.1029/94JD01028>, 1994.
- Koné, B., Diedhiou, A., Diawara, A., Anquetin, S., Bamba, A., Koba, A. T., et al.: Influence of initial soil moisture in a regional climate model study over West Africa–Part 2: Impact on the climate extremes, *Hydrology and Earth System Sciences*, 26, 731–754, <https://doi.org/10.5194/hess-26-731-2022>, 2022.
- 775 Lathiere, J., Hauglustaine, D., Friend, A., De Noblet-Ducoudré, N., Viovy, N., and Folberth, G.: Impact of climate variability and land use changes on global biogenic volatile organic compound emissions, *Atmospheric Chemistry and Physics*, 6, 2129–2146, <https://doi.org/10.5194/acp-6-2129-2006>, 2006.
- 780 Lavaysse, C., Flamant, C., Janicot, S., Parker, D. J., Lafore, J.-P., Sultan, B., and Pelon, J.: Seasonal evolution of the West African heat low: a climatological perspective, *Climate Dynamics*, 33, 313–330, <https://doi.org/10.1007/s00382-009-0553-4>, 2009.
- Lavaysse, C., Flamant, C., and Janicot, S.: Regional-scale convection patterns during strong and weak phases of the Saharan heat low, *Atmospheric Science Letters*, 11, 255–264, <https://doi.org/10.1002/asl.284>, 2010.
- Lavaysse, C., Chaboureaud, J.-P., and Flamant, C.: Dust impact on the West African heat low in summertime, *Quarterly Journal of the Royal Meteorological Society*, 137, 1227–1240, <https://doi.org/10.1002/qj.844>, 2011.
- 785 Lelieveld, J. and Dentener, F. J.: What controls tropospheric ozone?, *Journal of Geophysical Research: Atmospheres*, 105, 3531–3551, <https://doi.org/10.1029/1999JD901011>, 2000.
- Li, J., Nagashima, T., Kong, L., Ge, B., Yamaji, K., Fu, J. S., Wang, X., Fan, Q., Itahashi, S., Lee, H.-J., et al.: Model evaluation and inter-comparison of surface-level ozone and relevant species in East Asia in the context of MICS-Asia Phase III–Part 1: Overview, *Atmospheric Chemistry and Physics*, 19, 12 993–13 015, <https://doi.org/10.5194/acp-19-12993-2019>, 2019.
- 790 Li, R., Xu, M., Li, M., Chen, Z., Zhao, N., Gao, B., and Yao, Q.: Identifying the spatiotemporal variations in ozone formation regimes across China from 2005 to 2019 based on polynomial simulation and causality analysis, *Atmospheric Chemistry and Physics*, 21, 15 631–15 646, <https://doi.org/10.5194/acp-21-15631-2021>, 2021.
- Li, X., Yan, Y., Lu, X., Fu, L., and Liu, Y.: Responses of soil bacterial communities to precipitation change in the semi-arid alpine grassland of Northern Tibet, *Frontiers in Plant Science*, 13, 1036 369, <https://doi.org/10.3389/fpls.2022.1036369>, 2022.
- 795 Lin, H., Emmons, L. K., Lundgren, E. W., Yang, L. H., Feng, X., Dang, R., Zhai, S., Tang, Y., Kelp, M. M., Colombi, N. K., et al.: Intercomparison of GEOS-Chem and CAM-chem tropospheric oxidant chemistry within the Community Earth System Model version 2 (CESM2), *Atmospheric Chemistry and Physics*, 24, 8607–8624, <https://doi.org/10.5194/acp-24-8607-2024>, 2024.
- Lin, W., Xu, X., Yu, X., Zhang, X., and Huang, J.: Observed levels and trends of gaseous SO<sub>2</sub> and HNO<sub>3</sub> at Mt. Waliguan, China: Results from 1997 to 2009, *Journal of Environmental Sciences*, 25, 726–734, [https://doi.org/10.1016/S1001-0742\(12\)60143-0](https://doi.org/10.1016/S1001-0742(12)60143-0), 2013.
- 800 Liu, W., Zhang, Z., and Wan, S.: Predominant role of water in regulating soil and microbial respiration and their responses to climate change in a semiarid grassland, *Global Change Biology*, 15, 184–195, <https://doi.org/10.1111/j.1365-2486.2008.01728.x>, 2009.
- Liu, X., Xu, W., Du, E., Tang, A., Zhang, Y., Zhang, Y., Wen, Z., Hao, T., Pan, Y., Zhang, L., et al.: Environmental impacts of nitrogen emissions in China and the role of policies in emission reduction, *Philosophical Transactions of the Royal Society A*, 378, 20190 324, <https://doi.org/10.1098/rsta.2019.0324>, 2020.
- 805





- Lucas-Picher, P., Argüeso, D., Brisson, E., Trambly, Y., Berg, P., Lemonsu, A., Kotlarski, S., and Caillaud, C.: Convection-permitting modeling with regional climate models: Latest developments and next steps, *Wiley Interdisciplinary Reviews: Climate Change*, 12, e731, <https://doi.org/10.1002/wcc.731>, 2021.
- Ludwig, J., Meixner, F. X., Vogel, B., and Förstner, J.: Soil-air exchange of nitric oxide: An overview of processes, environmental factors, and modeling studies, *Biogeochemistry*, 52, 225–257, <https://doi.org/10.1023/A:1006424330555>, 2001.
- Mbienda, A. K., Guenang, G., Kaissassou, S., Tanessong, R., Choumbou, P., and Giorgi, F.: Enhancement of RegCM4. 7-CLM precipitation and temperature by improved bias correction methods over Central Africa, *Meteorological Applications*, 30, e2116, <https://doi.org/10.1002/met.2116>, 2023.
- McNally, A., Arsenault, K., Kumar, S., Shukla, S., Peterson, P., Wang, S., Funk, C., Peters-Lidard, C. D., and Verdin, J. P.: A land data assimilation system for sub-Saharan Africa food and water security applications, *Scientific data*, 4, 1–19, <https://doi.org/10.1038/sdata.2017.12>, 2017.
- McNally, A. et al.: FLDAS noah land surface model L4 global monthly  $0.1 \times 0.1$  degree (MERRA-2 and CHIRPS), *Atmos. Compos. Water Energy Cycles Clim. Var*, 2018.
- McNeill, A. and Unkovich, M.: The nitrogen cycle in terrestrial ecosystems, in: *Nutrient cycling in terrestrial ecosystems*, pp. 37–64, Springer, [https://doi.org/10.1007/978-3-540-68027-7\\_2](https://doi.org/10.1007/978-3-540-68027-7_2), 2007.
- Medinets, S., Skiba, U., Rennenberg, H., and Butterbach-Bahl, K.: A review of soil NO transformation: associated processes and possible physiological significance on organisms, *Soil Biology and Biochemistry*, 80, 92–117, <https://doi.org/10.1016/j.soilbio.2014.09.025>, 2015.
- Mosier, A. R.: Exchange of gaseous nitrogen compounds between agricultural systems and the atmosphere, *Plant and Soil*, 228, 17–27, <https://doi.org/10.1023/A:1004821205442>, 2001.
- Müller, J.-F.: Geographical distribution and seasonal variation of surface emissions and deposition velocities of atmospheric trace gases, *Journal of Geophysical Research: Atmospheres*, 97, 3787–3804, <https://doi.org/10.1029/91JD02757>, 1992.
- Nenes, A., Pandis, S. N., and Pilinis, C.: ISORROPIA: A new thermodynamic equilibrium model for multiphase multicomponent inorganic aerosols, *Aquatic geochemistry*, 4, 123–152, <https://doi.org/10.1023/A:1009604003981>, 1998.
- Nikulin, G., Jones, C., Giorgi, F., Asrar, G., Büchner, M., Cerezo-Mota, R., Christensen, O. B., Déqué, M., Fernandez, J., Hänsler, A., et al.: Precipitation climatology in an ensemble of CORDEX-Africa regional climate simulations, *Journal of Climate*, 25, 6057–6078, <https://doi.org/10.1175/JCLI-D-11-00375.1>, 2012.
- Nikulin, G., Kjellström, M. E., Hansson, U., Strandberg, G., and Ullerstig, A.: Evaluation and future projections of temperature, precipitation and wind extremes over Europe in an ensemble of regional climate simulations, *Tellus A: Dynamic Meteorology and Oceanography*, 63, 41–55, <https://doi.org/10.1111/j.1600-0870.2010.00466.x>, 2011.
- Nogherotto, R., Tompkins, A. M., Giuliani, G., Coppola, E., and Giorgi, F.: Numerical framework and performance of the new multiphase cloud microphysics scheme in RegCM4. 5: precipitation, cloud microphysics, and cloud radiative effects, *Geoscientific Model Development*, 9, 2533–2547, <https://doi.org/10.5194/gmd-9-2533-2016>, 2016.
- Oleson, K., Lawrence, D., Bonan, G., Drewniak, B., Huang, M., Koven, C., Levis, S., Li, F., Riley, W., Subin, Z., et al.: Technical description of version 4.5 of the Community Land Model (CLM), NCAR Earth System Laboratory–Climate and Global Dynamics Division, Boulder, Colorado, Tech. rep., USA, Tech. Rep. TN-503+ STR, <http://www.cesm.ucar.edu/models/cesm1.2/clm...>, 2013.
- Oppenheimer, C., Tsanev, V. I., Allen, A. G., McGonigle, A. J., Cardoso, A. A., Wiatr, A., Paterlini, W., and de Mello Dias, C.: NO<sub>2</sub> emissions from agricultural burning in Sao Paulo, Brazil, *Environmental science & technology*, 38, 4557–4561, <https://doi.org/10.1021/es0496219>, 2004.



- Ormeçi, B., Sanin, S. L., and Peirce, J. J.: Laboratory study of NO flux from agricultural soil: Effects of soil moisture, pH, and temperature, *Journal of Geophysical Research: Atmospheres*, 104, 1621–1629, <https://doi.org/10.1029/98JD02834>, 1999.
- 845 Ossohou, M., Galy-Lacaux, C., Yoboué, V., Hickman, J., Gardrat, E., Adon, M., Darras, S., Laouali, D., Akpo, A., Ouafu, M., et al.: Trends and seasonal variability of atmospheric NO<sub>2</sub> and HNO<sub>3</sub> concentrations across three major African biomes inferred from long-term series of ground-based and satellite measurements, *Atmospheric Environment*, 207, 148–166, <https://doi.org/10.1016/j.atmosenv.2019.03.027>, 2019.
- 850 Ossohou, M., Hickman, J. E., Clarisse, L., Coheur, P.-F., Van Damme, M., Adon, M., Yoboué, V., Gardrat, E., Alvès, M. D., and Galy-Lacaux, C.: Trends and seasonal variability in ammonia across major biomes in western and central Africa inferred from long-term series of ground-based and satellite measurements, *Atmospheric Chemistry and Physics*, 23, 9473–9494, <https://doi.org/10.5194/acp-23-9473-2023>, 2023.
- Pacifico, F., Delon, C., Jambert, C., Durand, P., Morris, E., Evans, M. J., Lohou, F., Derrien, S., Donnou, V. H., Houeto, A. V., et al.: Measurements of nitric oxide and ammonia soil fluxes from a wet savanna ecosystem site in West Africa during the DACCIWA field campaign, *Atmospheric Chemistry and Physics*, 19, 2299–2325, <https://doi.org/10.5194/acp-19-2299-2019>, 2019.
- 855 Padro, J., Den Hartog, G., and Neumann, H.: An investigation of the ADOM dry deposition module using summertime O<sub>3</sub> measurements above a deciduous forest, *Atmospheric Environment. Part A. General Topics*, 25, 1689–1704, [https://doi.org/10.1016/0960-1686\(91\)90027-5](https://doi.org/10.1016/0960-1686(91)90027-5), 1991.
- 860 Peyrillé, P., Lafore, J.-P., and Redelsperger, J.-L.: An idealized two-dimensional framework to study the West African monsoon. Part I: Validation and key controlling factors, *Journal of the atmospheric sciences*, 64, 2765–2782, <https://doi.org/10.1175/JAS3919.1>, 2007.
- Philippon, N., Cornu, G., Monteil, L., Gond, V., Moron, V., Pergaud, J., Sèze, G., Bigot, S., Camberlin, P., Doumenge, C., et al.: The light-deficient climates of western Central African evergreen forests, *Environmental Research Letters*, 14, 034007, <https://doi.org/10.1088/1748-9326/aaf5d8>, 2019.
- 865 Pichelli, E., Coppola, E., Sobolowski, S., Ban, N., Giorgi, F., Stocchi, P., Alias, A., Belušić, D., Berthou, S., Caillaud, C., et al.: The first multi-model ensemble of regional climate simulations at kilometer-scale resolution part 2: historical and future simulations of precipitation, *Climate Dynamics*, 56, 3581–3602, <https://doi.org/10.1007/s00382-021-05657-4>, 2021.
- Pilegaard, K.: Processes regulating nitric oxide emissions from soils, *Philosophical Transactions of the Royal Society B: Biological Sciences*, 368, 20130126, <https://doi.org/10.1098/rstb.2013.0126>, 2013.
- 870 Potter, P., Ramankutty, N., Bennett, E. M., and Donner, S. D.: Characterizing the spatial patterns of global fertilizer application and manure production, *Earth interactions*, 14, 1–22, <https://doi.org/10.1175/2009EI288.1>, 2010.
- Prein, A. F., Langhans, W., Fossier, G., Ferrone, A., Ban, N., Goergen, K., Keller, M., Tölle, M., Gutjahr, O., Feser, F., et al.: A review on regional convection-permitting climate modeling: Demonstrations, prospects, and challenges, *Reviews of geophysics*, 53, 323–361, <https://doi.org/10.1002/2014RG000475>, 2015.
- 875 Randerson, J., Van Der Werf, G., Giglio, L., Collatz, G., and Kasibhatla, P.: Global Fire Emissions Database, Version 4.1 (GFEDv4), ORNL DAAC, Oak Ridge, Tennessee, USA, <https://doi.org/10.3334/ORNLDAAAC/1293>, 2018.
- Rao, P., Wang, Y., Wang, F., Liu, Y., Wang, X., and Wang, Z.: Daily soil moisture mapping at 1 km resolution based on SMAP data for desertification areas in northern China, *Earth System Science Data*, 14, 3053–3073, <https://doi.org/10.5194/essd-14-3053-2022>, 2022.
- Roelle, P. A., Aneja, V. P., Gay, B., Geron, C., and Pierce, T.: Biogenic nitric oxide emissions from cropland soils, *Atmospheric Environment*, 880 35, 115–124, [https://doi.org/10.1016/S1352-2310\(00\)00279-X](https://doi.org/10.1016/S1352-2310(00)00279-X), 2001.



- Sanhueza, E., Hao, W. M., Scharffe, D., Donoso, L., and Crutzen, P. J.: N<sub>2</sub>O and NO emissions from soils of the northern part of the Guayana Shield, Venezuela, *Journal of Geophysical Research: Atmospheres*, 95, 22 481–22 488, <https://doi.org/10.1029/JD095iD13p22481>, 1990.
- Sauvage, B., Thouret, V., Cammas, J.-P., Gheusi, F., Athier, G., and Nédélec, P.: Tropospheric ozone over Equatorial Africa: regional aspects from the MOZAIK data, *Atmospheric Chemistry and Physics*, 5, 311–335, <https://doi.org/10.5194/acp-5-311-2005>, 2005.
- 885 Sauvage, B., Martin, R. V., Van Donkelaar, A., and Ziemke, J.: Quantification of the factors controlling tropical tropospheric ozone and the South Atlantic maximum, *Journal of Geophysical Research: Atmospheres*, 112, <https://doi.org/10.1029/2006JD008008>, 2007.
- Schreiber, F., Wunderlin, P., Udert, K. M., and Wells, G. F.: Nitric oxide and nitrous oxide turnover in natural and engineered microbial communities: biological pathways, chemical reactions, and novel technologies, *Frontiers in microbiology*, 3, 372, <https://doi.org/10.3389/fmicb.2012.00372>, 2012.
- 890 Serca, D., Delmas, R., Jambert, C., and Labroue, L.: Emissions of nitrogen oxides from equatorial rain forest in central Africa, *Tellus B: Chemical and Physical Meteorology*, 46, 243–254, <https://doi.org/10.3402/tellusb.v46i4.15795>, 1994.
- Shalaby, A., Zakey, A., Tawfik, A., Solmon, F., Giorgi, F., Stordal, F., Sillman, S., Zaveri, R. A., and Steiner, A.: Implementation and evaluation of online gas-phase chemistry within a regional climate model (RegCM-CHEM4), *Geoscientific Model Development*, 5, 741–760, <https://doi.org/10.5194/gmd-5-741-2012>, 2012.
- 895 Sillman, S. and He, D.: Some theoretical results concerning O<sub>3</sub>-NO<sub>x</sub>-VOC chemistry and NO<sub>x</sub>-VOC indicators, *Journal of Geophysical Research: Atmospheres*, 107, ACH–26, <https://doi.org/10.1029/2001JD001123>, 2002.
- Simpson, D. and Darras, S.: Global soil no emissions for atmospheric chemical transport modelling: Cams-glob-soil v2. 2, *Earth System Science Data Discussions*, 2021, 1–35, <https://doi.org/10.5194/essd-2021-221>, 2021.
- Skopp, J., Jawson, M., and Doran, J.: Steady-state aerobic microbial activity as a function of soil water content, *Soil Science Society of America Journal*, 54, 1619–1625, <https://doi.org/10.2136/sssaj1990.03615995005400060018x>, 1990.
- 900 Solmon, F., Giorgi, F., and Lioussé, C.: Aerosol modelling for regional climate studies: application to anthropogenic particles and evaluation over a European/African domain, *Tellus B: Chemical and Physical Meteorology*, 58, 51–72, <https://doi.org/10.1111/j.1600-0889.2005.00155.x>, 2006.
- Solmon, F., Elguindi, N., Mallet, M., Flamant, C., and Formenti, P.: West African monsoon precipitation impacted by the South Eastern Atlantic biomass burning aerosol outflow, *npj climate and atmospheric science*, 4, 54, <https://doi.org/10.1038/s41612-021-00210-w>, 2021.
- 905 Soulie, A., Granier, C., Darras, S., Zilbermann, N., Doumbia, T., Guevara, M., Jalkanen, J.-P., Keita, S., Lioussé, C., Crippa, M., et al.: Global anthropogenic emissions (CAM5-GLOB-ANT) for the Copernicus Atmosphere Monitoring Service simulations of air quality forecasts and reanalyses, *Earth System Science Data Discussions*, 2023, 1–45, <https://doi.org/10.5194/essd-16-2261-2024>, 2023.
- Stehfest, E. and Bouwman, L.: N<sub>2</sub>O and NO emission from agricultural fields and soils under natural vegetation: summarizing available measurement data and modeling of global annual emissions, *Nutrient cycling in agroecosystems*, 74, 207–228, <https://doi.org/10.1007/s10705-006-9000-7>, 2006.
- 910 Steinkamp, J. and Lawrence, M. G.: Improvement and evaluation of simulated global biogenic soil NO emissions in an AC-GCM, *Atmospheric Chemistry and Physics*, 11, 6063–6082, <https://doi.org/10.5194/acp-11-6063-2011>, 2011.
- Steinkamp, J., Ganzeveld, L., Wilcke, W., and Lawrence, M.: Influence of modelled soil biogenic NO emissions on related trace gases and the atmospheric oxidizing efficiency, *Atmospheric Chemistry and Physics*, 9, 2663–2677, <https://doi.org/10.5194/acp-9-2663-2009>, 2009.
- 915 Stewart, D., Taylor, C., Reeves, C., and McQuaid, J.: Biogenic nitrogen oxide emissions from soils: impact on NO<sub>x</sub> and ozone over west Africa during AMMA (African Monsoon Multidisciplinary Analysis): observational study, *Atmospheric Chemistry and Physics*, 8, 2285–2297, <https://doi.org/10.5194/acp-8-2285-2008>, 2008.



- Stohl, A., Williams, E., Wotawa, G., and Kromp-Kolb, H.: A European inventory of soil nitric oxide emissions and the effect of these emis-  
920 sions on the photochemical formation of ozone, *Atmospheric environment*, 30, 3741–3755, [https://doi.org/10.1016/1352-2310\(96\)00104-5](https://doi.org/10.1016/1352-2310(96)00104-5), 1996.
- Strada, S., Pozzer, A., Giuliani, G., Coppola, E., Solmon, F., Jiang, X., Guenther, A., Bourtsoukidis, E., Serça, D., Williams, J., et al.:  
Assessment of isoprene and near-surface ozone sensitivities to water stress over the Euro-Mediterranean region, *Atmospheric Chemistry  
and Physics*, 23, 13 301–13 327, <https://doi.org/10.5194/acp-23-13301-2023>, 2023.
- 925 Sultan, B., Janicot, S., and Diedhiou, A.: The West African monsoon dynamics. Part I: Documentation of intraseasonal variability, *Journal  
of Climate*, 16, 3389–3406, [https://doi.org/10.1175/1520-0442\(2003\)016<3389:TWAMDP>2.0.CO;2](https://doi.org/10.1175/1520-0442(2003)016<3389:TWAMDP>2.0.CO;2), 2003.
- Sun, S., Tai, A. P., Yung, D. H., Wong, A. Y., Ducker, J. A., and Holmes, C. D.: Influence of plant ecophysiology on ozone dry deposition:  
comparing between multiplicative and photosynthesis-based dry deposition schemes and their responses to rising CO<sub>2</sub> level, *Biogeo-  
sciences*, 19, 1753–1776, <https://doi.org/10.5194/bg-19-1753-2022>, 2022.
- 930 Sylla, M., Giorgi, F., and Stordal, F.: Large-scale origins of rainfall and temperature bias in high-resolution simulations over southern Africa,  
*Climate Research*, 52, 193–211, <https://doi.org/10.3354/cr01044>, 2012.
- Sylla, M., Diallo, I., and Pal, J.: West African monsoon in state-of the-art regional climate models, <https://doi.org/10.5772/55140>, 2013b.
- Tadic, I., Nussbaumer, C. M., Bohn, B., Harder, H., Marno, D., Martinez, M., Obersteiner, F., Parchatka, U., Pozzer, A., Rohloff, R., et al.:  
Central role of nitric oxide in ozone production in the upper tropical troposphere over the Atlantic Ocean and western Africa, *Atmospheric  
935 Chemistry and Physics*, 21, 8195–8211, <https://doi.org/10.5194/acp-21-8195-2021>, 2021.
- Tadross, M., Gutowski, W., Hewitson, B., Jack, C., and New, M.: MM5 simulations of interannual change and the diurnal cycle of southern  
African regional climate, *Theoretical and Applied Climatology*, 86, 63–80, <https://doi.org/10.1007/s00704-005-0208-2>, 2006.
- Tiedtke, M.: A comprehensive mass flux scheme for cumulus parameterization in large-scale models, *Monthly weather review*, 117, 1779–  
1800, [https://doi.org/10.1175/1520-0493\(1989\)117<1779:ACMFSF>2.0.CO;2](https://doi.org/10.1175/1520-0493(1989)117<1779:ACMFSF>2.0.CO;2), 1989.
- 940 Tsivlidou, M., Sauvage, B., Bennouna, Y., Blot, R., Boulanger, D., Clark, H., Le Flochmoën, E., Nédélec, P., Thouret, V., Wolff, P., et al.:  
Tropical tropospheric ozone and carbon monoxide distributions: characteristics, origins, and control factors, as seen by IAGOS and IASI,  
*Atmospheric Chemistry and Physics*, 23, 14 039–14 063, <https://doi.org/10.5194/acp-23-14039-2023>, 2023.
- Valari, M. and Menut, L.: Does an increase in air quality models’ resolution bring surface ozone concentrations closer to reality?, *Journal of  
Atmospheric and Oceanic Technology*, 25, 1955–1968, <https://doi.org/10.1175/2008JTECHA1123.1>, 2008.
- 945 Van Der A, R., Eskes, H., Boersma, K., Van Noije, T., Van Roozendaal, M., De Smedt, I., Peters, D., and Meijer, E.: Trends, seasonal  
variability and dominant NO<sub>x</sub> source derived from a ten year record of NO<sub>2</sub> measured from space, *Journal of Geophysical Research:  
Atmospheres*, 113, <https://doi.org/10.1029/2007JD009021>, 2008.
- Van Marle, M. J., Kloster, S., Magi, B. I., Marlon, J. R., Daniau, A.-L., Field, R. D., Arneeth, A., Forrest, M., Hantson, S., Kehrwald, N. M.,  
et al.: Historic global biomass burning emissions for CMIP6 (BB4CMIP) based on merging satellite observations with proxies and fire  
950 models (1750–2015), *Geoscientific Model Development*, 10, 3329–3357, <https://doi.org/10.5194/gmd-10-3329-2017>, 2017.
- Vinken, G., Boersma, K., Maasackers, J., Adon, M., and Martin, R.: Worldwide biogenic soil NO<sub>x</sub> emissions inferred from OMI NO<sub>2</sub>  
observations, *Atmospheric Chemistry and Physics*, 14, 10 363–10 381, <https://doi.org/10.5194/acp-14-10363-2014>, 2014.
- Vitousek, P. M., Aber, J. D., Howarth, R. W., Likens, G. E., Matson, P. A., Schindler, D. W., Schlesinger, W. H., and Tilman, D. G.: Human  
alteration of the global nitrogen cycle: sources and consequences, *Ecological applications*, 7, 737–750, [https://doi.org/10.1890/1051-  
0761\(1997\)007\[0737:HAOTGN\]2.0.CO;2](https://doi.org/10.1890/1051-<br/>955 0761(1997)007[0737:HAOTGN]2.0.CO;2), 1997.



- Wagner, A., Bennouna, Y., Blechschmidt, A.-M., Brasseur, G., Chabrilat, S., Christophe, Y., Errera, Q., Eskes, H., Flemming, J., Hansen, K., et al.: Comprehensive evaluation of the Copernicus Atmosphere Monitoring Service (CAMS) reanalysis against independent observations: Reactive gases, *Elem Sci Anth*, 9, 00 171, <https://doi.org/10.1525/elementa.2020.00171>, 2021.
- Wang, W., Sheng, L., Jin, H., and Han, Y.: Dust aerosol effects on cirrus and altocumulus clouds in Northwest China, *Journal of Meteorological Research*, 29, 793–805, <https://doi.org/10.1007/s13351-015-4116-9>, 2015.
- Wang, Y., Ma, Y.-F., Muñoz-Esparza, D., Dai, J., Li, C. W. Y., Lichtig, P., Tsang, R. C.-W., Liu, C.-H., Wang, T., and Brasseur, G. P.: Coupled mesoscale–microscale modeling of air quality in a polluted city using WRF-LES-Chem, *Atmospheric Chemistry and Physics*, 23, 5905–5927, <https://doi.org/10.5194/acp-23-5905-2023>, 2023.
- Williams, E., Guenther, A., and Fehsenfeld, F.: An inventory of nitric oxide emissions from soils in the United States, *Journal of Geophysical Research: Atmospheres*, 97, 7511–7519, <https://doi.org/10.1029/92JD00412>, 1992.
- Williams, J., Scheele, M., van Velthoven, P., Cammas, J.-P., Thouret, V., Galy-Lacaux, C., and Volz-Thomas, A.: The influence of biogenic emissions from Africa on tropical tropospheric ozone during 2006: a global modeling study, *Atmospheric Chemistry and Physics*, 9, 5729–5749, <https://doi.org/10.5194/acp-9-5729-2009>, 2009.
- Wu, Z., Wang, X., Chen, F., Turnipseed, A. A., Guenther, A. B., Niyogi, D., Charusombat, U., Xia, B., Munger, J. W., and Alapaty, K.: Evaluating the calculated dry deposition velocities of reactive nitrogen oxides and ozone from two community models over a temperate deciduous forest, *Atmospheric Environment*, 45, 2663–2674, <https://doi.org/10.1016/j.atmosenv.2011.02.063>, 2011.
- Yan, X., Ohara, T., and Akimoto, H.: Statistical modeling of global soil NO<sub>x</sub> emissions, *Global Biogeochemical Cycles*, 19, <https://doi.org/10.1029/2004GB002276>, 2005.
- Yienger, J. and Levy, H.: Empirical model of global soil-biogenic NO<sub>x</sub> emissions, *Journal of Geophysical Research: Atmospheres*, 100, 11 447–11 464, <https://doi.org/10.1029/95JD00370>, 1995.
- Young, P. J., Naik, V., Fiore, A. M., Gaudel, A., Guo, J., Lin, M., Neu, J., Parrish, D., Rieder, H., Schnell, J., et al.: Tropospheric Ozone Assessment Report: Assessment of global-scale model performance for global and regional ozone distributions, variability, and trends, *Elem Sci Anth*, 6, 10, <https://doi.org/10.1525/elementa.265>, 2018.
- Zaveri, R. A. and Peters, L. K.: A new lumped structure photochemical mechanism for large-scale applications, *Journal of Geophysical Research: Atmospheres*, 104, 30 387–30 415, <https://doi.org/10.1029/1999JD900876>, 1999.
- Zhang, L., Moran, M. D., Makar, P. A., Brook, J. R., and Gong, S.: Modelling gaseous dry deposition in AURAMS: a unified regional air-quality modelling system, *Atmospheric Environment*, 36, 537–560, [https://doi.org/10.1016/S1352-2310\(01\)00447-2](https://doi.org/10.1016/S1352-2310(01)00447-2), 2002.
- Zhang, L., Brook, J. R., and Vet, R.: A revised parameterization for gaseous dry deposition in air-quality models, *Atmospheric Chemistry and Physics*, 3, 2067–2082, <https://doi.org/10.5194/acp-3-2067-2003>, 2003.
- Zittis, G., Hadjinicolaou, P., Fnais, M., and Lelieveld, J.: Projected changes in heat wave characteristics in the eastern Mediterranean and the Middle East, *Regional environmental change*, 16, 1863–1876, <https://doi.org/10.1007/s10113-014-0753-2>, 2016.

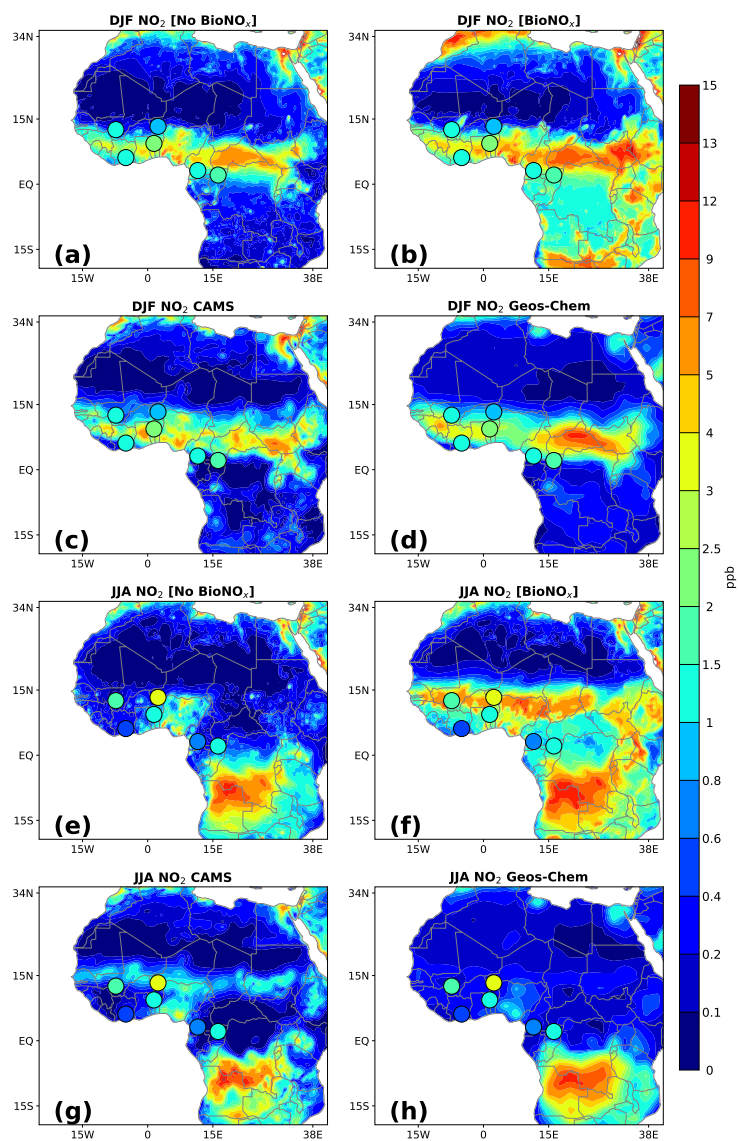


**Figure 6.** Comparison of BASE and BioNO simulations of surface NO<sub>2</sub> against the CAMS reanalysis and the Geos-Chem model for DJF and JJA seasons. The INDAAF measurement values are overlotted and represented by small circles on the map.



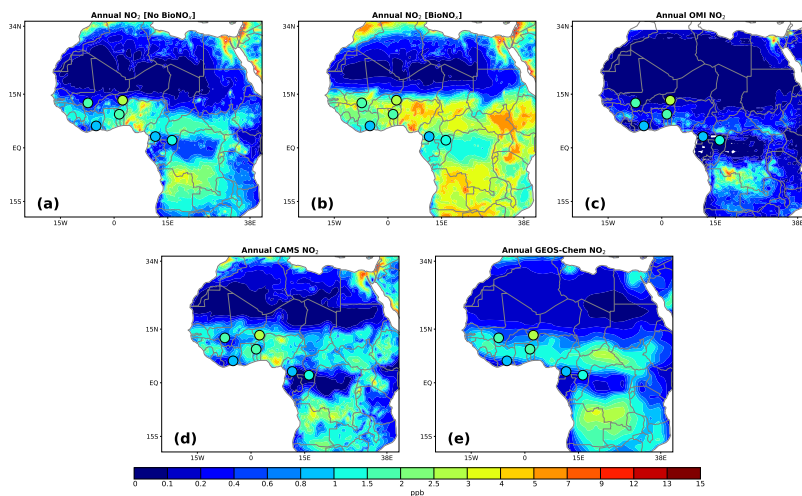


**Figure 7.** Comparison of BASE and BioNO simulations of annual mean surface NO<sub>2</sub> concentrations (ppb) against OMI and TROPOMI-derived surface-level concentrations over 2010-2013, the CAMS reanalysis and the GEOS-Chem model. The INDAAF measurement values are overplotted and represented by small circles on the map.

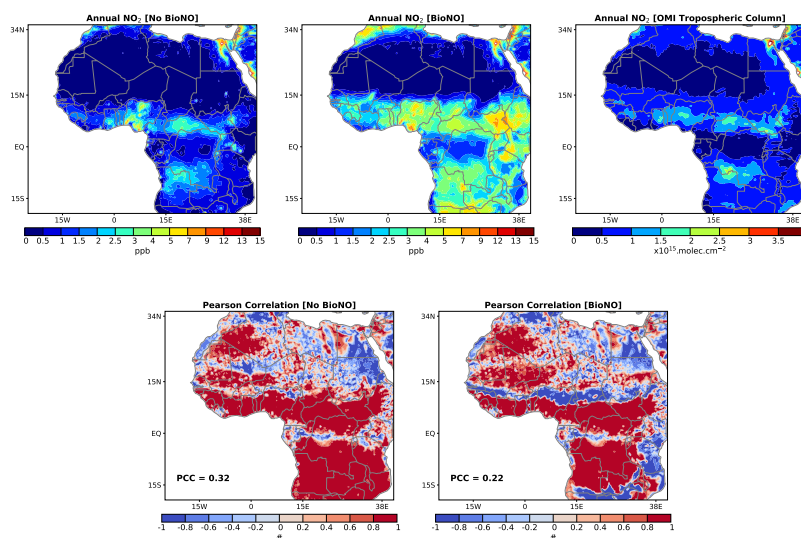


**Figure 8.** Comparison of BASE and BIONO simulations of annual mean surface NO<sub>2</sub> concentrations (ppb) against OMI and OMI/Aura-derived tropospheric NO<sub>2</sub> columns over 2010-2013, and associated Pearson spatial correlation.

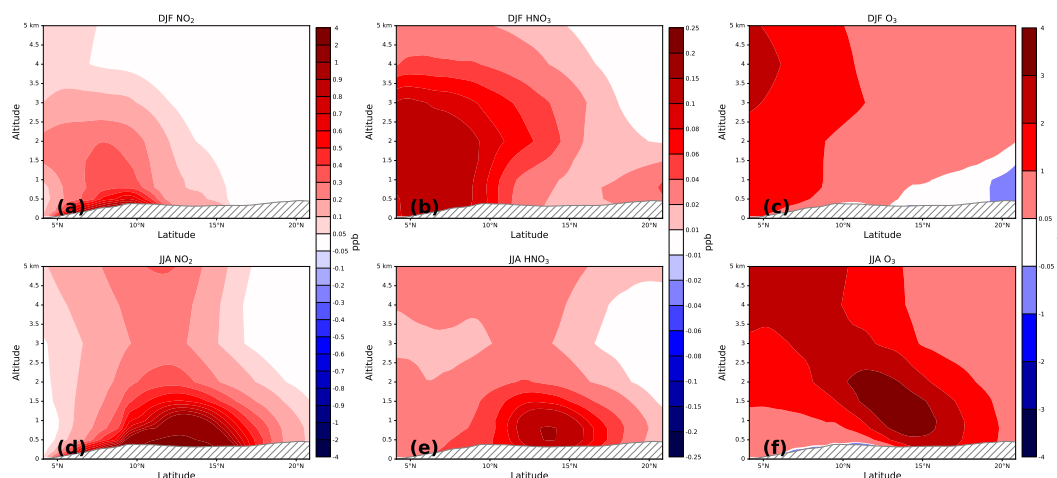


**Figure 9.** DJF and JJA differences (BIONO - BASE) in NO<sub>2</sub> (a, d), HNO<sub>3</sub> (d, e) and O<sub>3</sub> (c, f) concentrations, on the transect 4-21°N averaged between 10°W-10°E. Units are in ppb.

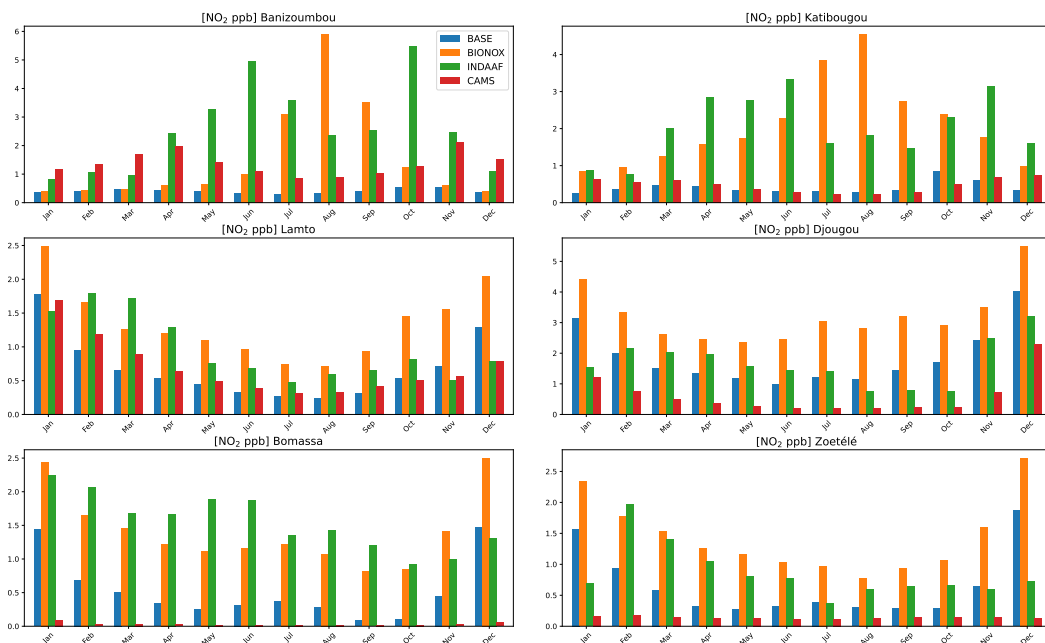


**Figure 10.** Simulated monthly-averaged concentrations of  $\text{NO}_2$  by BASE, BIONOX runs and the CAMS reanalysis in comparison with INDAAF observation at representative remote sites.

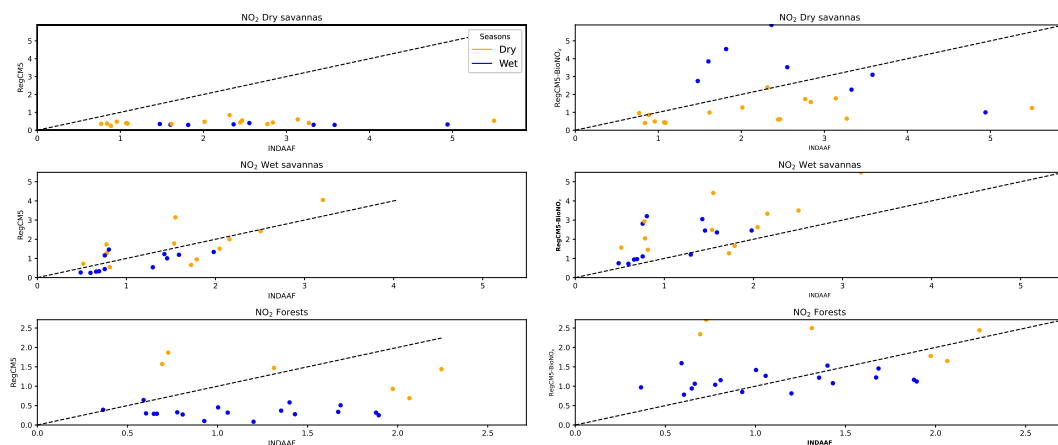


**Figure 11.** Surface observed  $\text{NO}_2$  concentrations (INDAAF) vs simulated with RegCM5. BioNO emissions are considered in the right panel.

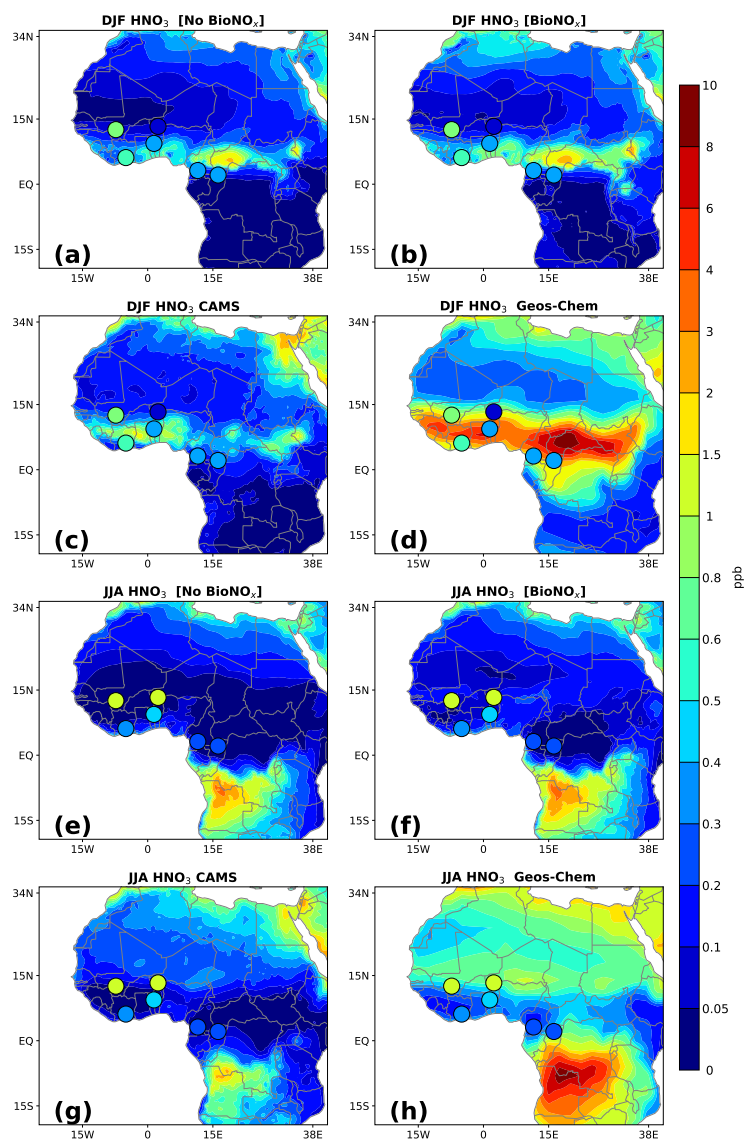


**Figure 12.** Comparison of BASE and BioNO simulations of surface  $\text{HNO}_3$  concentrations (in ppb) against the CAMS reanalysis and the model Geos-Chem for DJF and JJA season. The INDAAF measurement values are overlotted and represented by small circles on the map

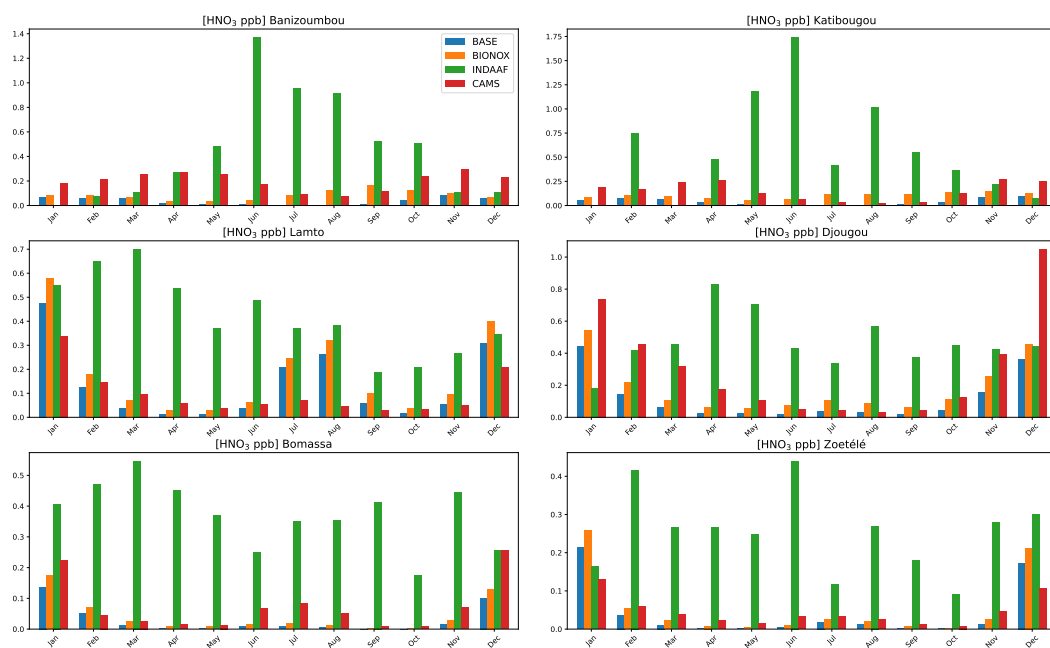


**Figure 13.** Simulated monthly-averaged concentrations of HNO<sub>3</sub> by BASE, BIONOX runs and the CAMS reanalysis in comparison with INDAAF observation at its representative remote sites.

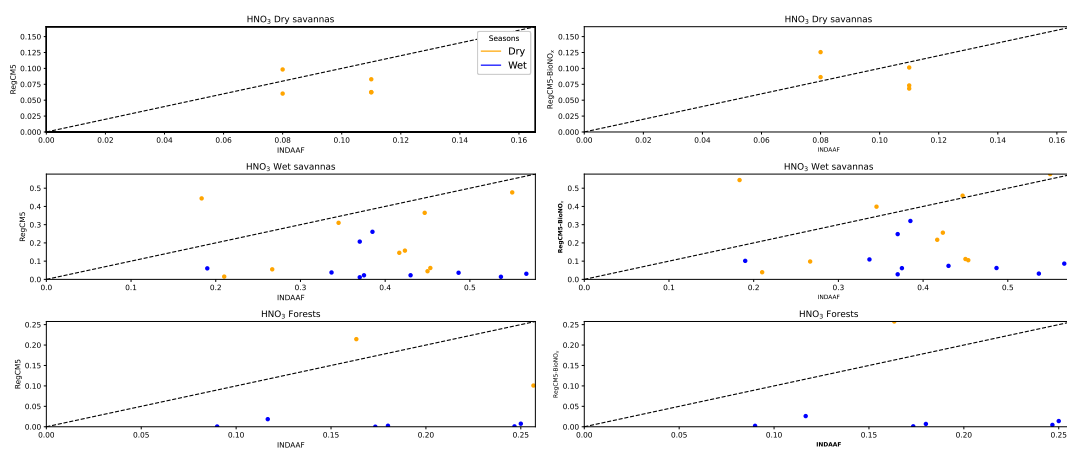


**Figure 14.** Surface observed  $\text{HNO}_3$  concentrations (INDAAF) vs simulated with RegCM5.  $\text{BiONO}_2$  emissions are considered in the right panel.



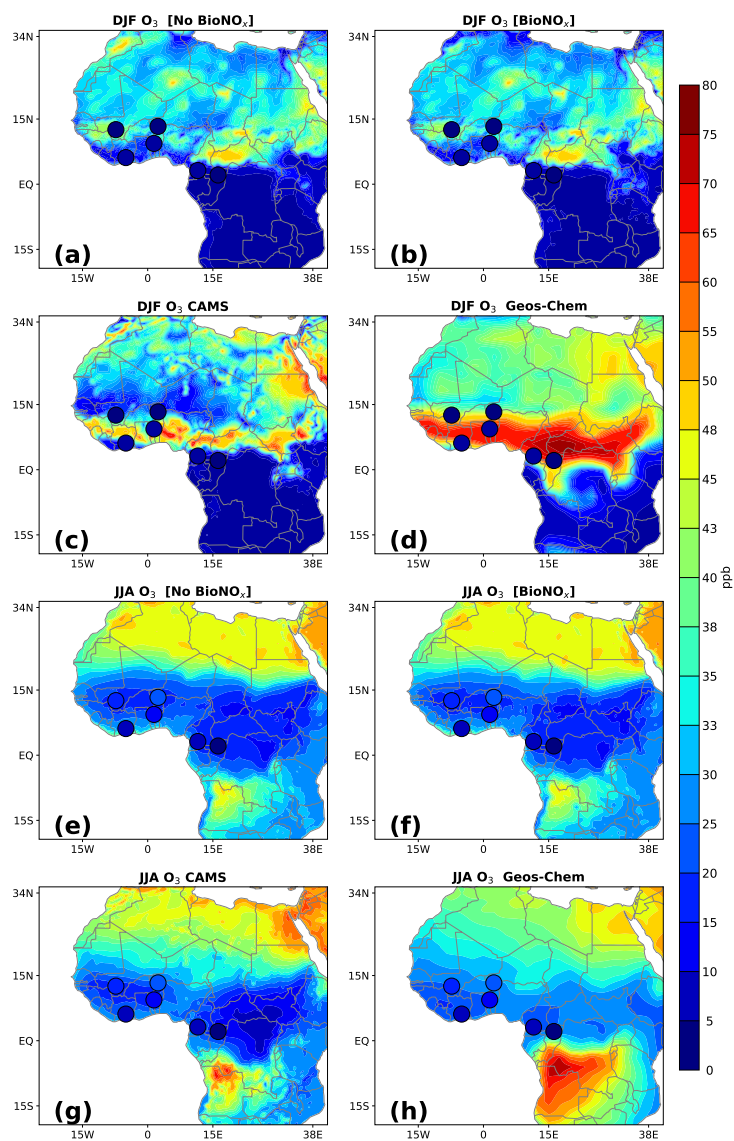


**Figure 15.** Comparison of BASE and BioNO simulations of surface O<sub>3</sub> concentrations (in ppb) against the CAMS reanalysis and the model Geos-Chem for DJF and JJA season. The INDAAF measurement values are overlotted and represented by small circles on the map.

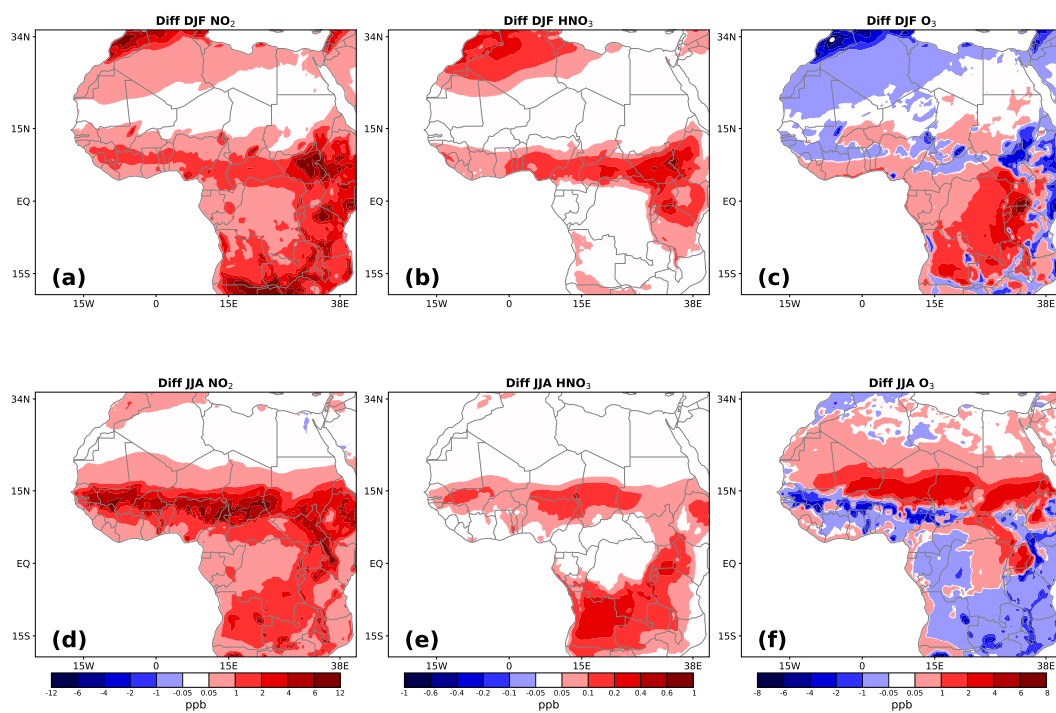


**Figure 16.** DJA and JJA differences (BIONO - BASE) in surface NO<sub>2</sub> (left), HNO<sub>3</sub> (middle) and O<sub>3</sub> (right) concentrations. Units are in ppb.

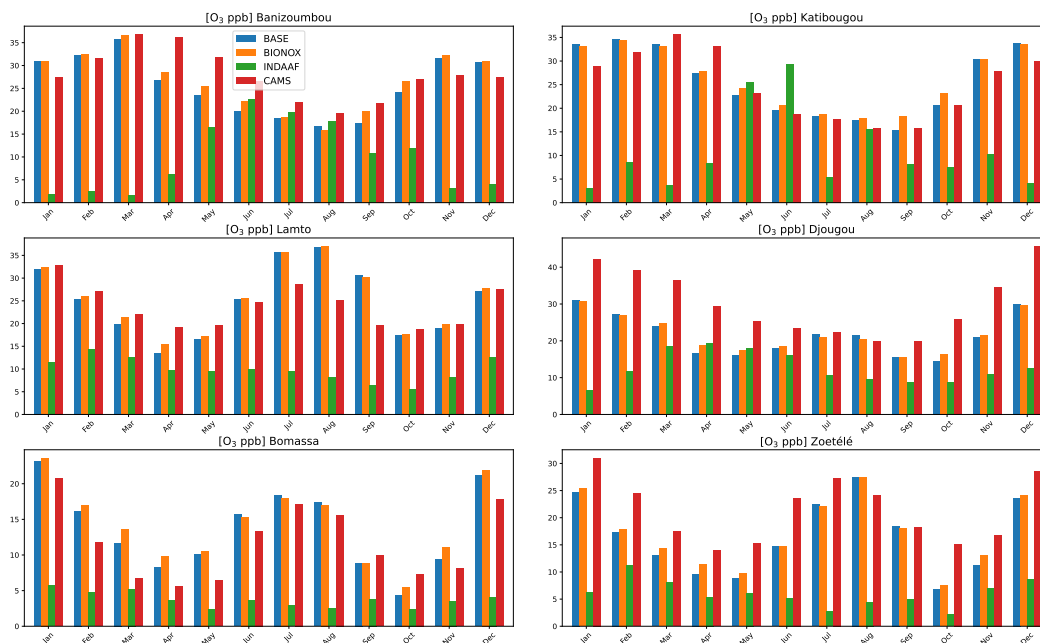


**Figure 17.** Simulated monthly-averaged concentrations of O<sub>3</sub> by BASE, BIONOX runs and the CAMS reanalysis in comparison with INDAAF observation at its representative remote sites.

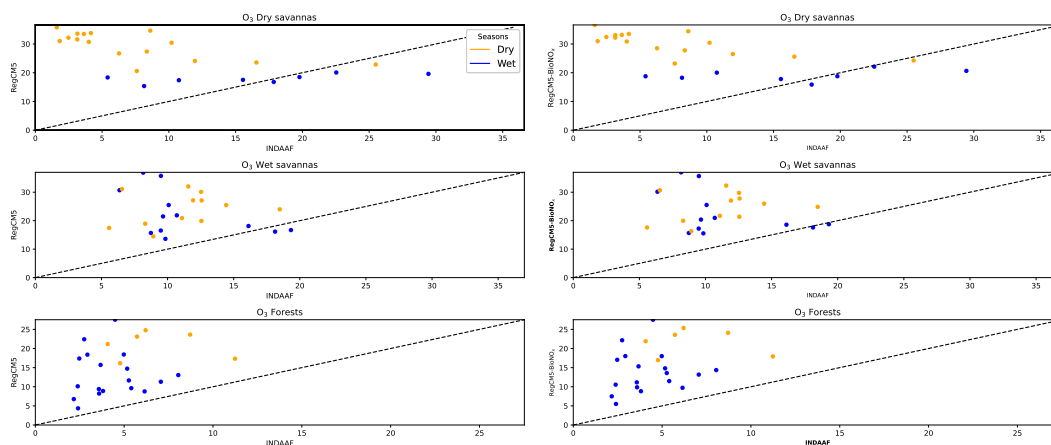


**Figure 18.** Surface observed O<sub>3</sub> concentrations (INDAAF) vs simulated with RegCM5. BioNO emissions are considered in the right panel.